THS



This is to certify that the

thesis entitled

Design and Performance of an Ultrasonic Phased Array Tranducer

presented by

Usman Saeed

has been accepted towards fulfillment of the requirements for

<u>Masters</u> degree in <u>Electrical</u>
Engineering and Systems Science

Donnie K. Reinhard

Donnie K Reishard

Major professor

Date 2/22/78

O-7639

APR 2 4 2005

DESIGN AND PERFORMANCE OF AN ULTRASONIC PHASED ARRAY TRANSDUCER

Ву

Usman Saeed

A THESIS

Submitted to
Michigan State University
in partial fulfillment of the requirements
for the degree of

MASTER OF SCIENCE

Department of Electrical Engineering and Systems Science

1978

5.1135 AV

ABSTRACT

DESIGN AND PERFORMANCE OF AN ULTRASONIC PHASED ARRAY TRANSDUCER

Ву

Usman Saeed

An ultrasonic transducer phased array has been designed, fabricated and tested for the purpose of investigating the potential advantages and problems of incorporating such a transducer in a computerized ultrasonic imaging system.

The fabrication was preceded by computer calculations based on a theoretical model. The performance testing of the ultrasonic phased array is based on the study of field strength patterns of individual elements as well as the array itself. For testing the ultrasonic beam steering capabilities of the fabricated transducer array, a programmable delay line has been developed, which can provide the necessary delays for each of the elements of the array to produce a constructive interference pattern at the target point.

Several experiments were performed by observing the field strength pattern of an individual central element and the seven element array under different operating conditions. Results lead to the conclusion that indeed an ultrasonic phased array can be fabricated by the method used during this research. Both beam steering and focusing were performed successfully, however, several important differences between observations and predictions were noted; notably reduced lateral resolution and dynamic range. Some suggestions for resolving these differences are discussed.

ACKNOWLEDGMENTS

I am deeply indebted to my research advisor, Dr. D. K. Reinhard, for his invaluable advice, guidance and encouragement which he rendered during the course of this research. His sound technical advise and enthusiasm helped me in completing this research.

I would like to extend special thanks to Dr. E. James Potchen, Chairman of the Radiology Department, for his keen interest towards this research and to the Biomedical Research Support Group which financed a part of this research along with the Radiology Department at Michigan State University.

Special appreciation is extended to my major professors, Dr. G. L. Park and Dr. R. O. Barr, for their thorough review of the thesis.

I would also like to extend my sincere thanks to Dr. G. Harris, Mr. Philip Chimento, Mr. Bruce Johnston, Mr. David Gift, Mr. James Siebert and my fellow research assistant, Mr. Mark Funk, for their supportive efforts in this project.

TABLE OF CONTENTS

Chapter		Page
I.	INTRODUCTION	1
II.	THEORY OF PHASED ARRAYS	
	2.1 Field Strength Expression for an Array2.2 Beam Steering2.3 Beam Focusing2.4 Expressions for a Circular Element	8 16 19
	Transducer	23
	2.5 Expressions for a Rectangular Element Array	25
III.	ULTRASONIC PHASED ARRAY FABRICATION	28
IV.	EXPERIMENTAL RESULTS	
	4.1 Group 1 Experiments	33 39
٧.	CROSS COUPLING	56
	5.1 Experimental Results	63
VI.	CONCLUSIONS	66
VII.	RECOMMENDATIONS	70
	REFERENCES	71
	APPENDICES	
	A. Programmable Delay Line B. Gates and Power Amplifiers C. Computer Programs	73 77 81

LIST OF TABLES

Table		Page
1.	Computer Simulation of Field Strength Pattern of an Array	12
2.	Computer Simulation of Field Strength Pattern of an Array Element	14
3.	Computer Simulation of Field Strength Pattern on Steering	19
4.	Computer Simulation of Field Strength Pattern on Focusing	23
5.	Output Voltage versus Axial Displacement of an Array	37
6.	Output Voltage versus Axial Displacement of an Array Element	39
7.	Output Voltage versus Axial Displacement of an Array	43
8.	Output Voltage versus Axial Displacement of an Array Element	45
9.	Vout versus Axial Displacement for Left Side Beam Steering	47
10.	Vout versus Axial Displacement for Right Side Beam Steering	48
11.	Vout versus Axial Displacement for Left Side Beam Steering	52
12.	Vout versus Axial Displacement for Left Side Beam Steering	53
13.	Induced Voltage for Different Elements of the Array	64

Table		Page
14.	Induced Voltage for Different Elements of the Array	65
15.	Induced Voltage for Different Elements of the Array	65

LIST OF FIGURES

Figure		Page
1.	System Block Diagram	3
2.	Geometrical Details of an Array	9
3.	Simulation Plot of $P(\theta)$ vs θ for an Array	13
4.	Simulation Plot of $P(\theta)$ vs θ for an Array Element	15
5.	Simulation Plot of $P(\theta)$ vs θ on Steering	18
6.	Focusing Effect	20
. 7.	Simulation Plot of $P(\theta)$ vs θ on Focusing	24
8.	Rectangular Element Array	27
9.	Fabrication Details for Transducer	30
10.	Controlling Electronics of Group 1 Experiments	34
11.	Plot of Vout vs Axial Displacement of an Array	36
12.	Plot of Vout vs Axial Displacement of an Array Element	38
13.	Controlling Electronics of Group 2 Experiments	40
14.	Plot of Vout vs Axial Displacement of an Array	42
15.	Plot of Vout vs Axial Displacement of an Array Element	44
16.	Plot of Vout vs Axial Displacement for Left Side Beam Steering	46
17.	Plot of Vout vs Axial Displacement for Right Side Beam Steering	49
18.	Plot of Vout vs Axial Displacement for Left Side Beam Steering	51

Figure		Page
19.	Plot of Vout vs Axial Displacement for Left Side Beam Steering	54
20.	Equivalent Circuit Model of an Array Element	58
21.	Norton's Equivalent Model of an Array Element	58
22.	Receiving Element Equivalent Circuit	60
23.	Plane Wave Model of a Transmitting/ Receiving Element of an Array	62
24.	Programmable Delay Line	74
25.	Block Diagram of Gates and Power Amplifier	78
26.	Circuit Diagram of Power Amplifier	80

CHAPTER I INTRODUCTION

Ultrasound has been used for the past three decades as an alternative or as a complementary technique to x-rays for medical diagnostic examinations. (1) Inhomogeneities in a medium may be determined and imaged by observation of reflected ultrasound waves, for example flaw detection in metallic plates, sonar, etc. More recently, phased arrays have been used to advantage as ultrasound transducers since the ultrasound waves may be electronically steered and focused. (2)

This thesis deals with the fabrication, theory and performance testing of phased array ultrasound transducers. The need for a study of ultrasonic phased arrays arose in order to investigate the potential advantages of electronic beam steering and focusing for the computerized ultrasonic system being developed in the Radiology Department of Michigan State University.

Ultrasound transducers are used for generating mechanical stress waves when excited by a pulsed electric field. If the transducer is coupled to a medium, ultrasound energy is transmitted to the medium in the form of waves. Commonly, the active element of the ultrasound transducer is a solid state crystalline or polycrystalline piezoelectric such as lead zirconate. In the polycrysalline form, these materials are made in the form of a ceramic composed of a large number of randomly oriented polarized domains. When such materials are heated and then cooled in the presence of a strong electric field, the direction of polarization of these domains line up with the field and

remain lined up even after the field is removed. If a certain mechanical stress is applied on such materials, it is their inherent characteristic to develop a certain charge on the surface. This phenomona is called the piezoelectric effect. (3) Conversely, if a voltage is applied between the two faces of such a material it will cause a mechanical deformation and generate a mechanical stress wave. This phenomona is called the inverse piezoelectric effect.

The mechanical stress waves are longitudinal in nature. Their velocity in a given medium depends upon the density of the medium and its elasticity. (4) When an obstruction comes in the path of an ultrasound wave, part of it passes through the boundary but a part of it gets reflected back. This happens with every boundary the wave meets. An image of the obstructing object's boundaries can be created if one is able to detect these reflections. This principle is used frequently in medical diagnosis equipment using ultrasound transducers. An important feature of ultrasound waves is that it is a non-ionizing radiation, and hence it is non-carcinogenic. This makes them presumably safer than x-rays.

This research was a part of an investigation being carried out at the Radiology Department at Michigan State University which may be described as "computer control and processing of ultrasound signals for clinical application."

The overall block diagram of the total system where this particular research fits in is shown in Figure 1 and is described in brief as follows:

 The transducer is made in the form of an array rather than a single element. This gives it the feature of electronically steering and focusing the beam. The system may also be used

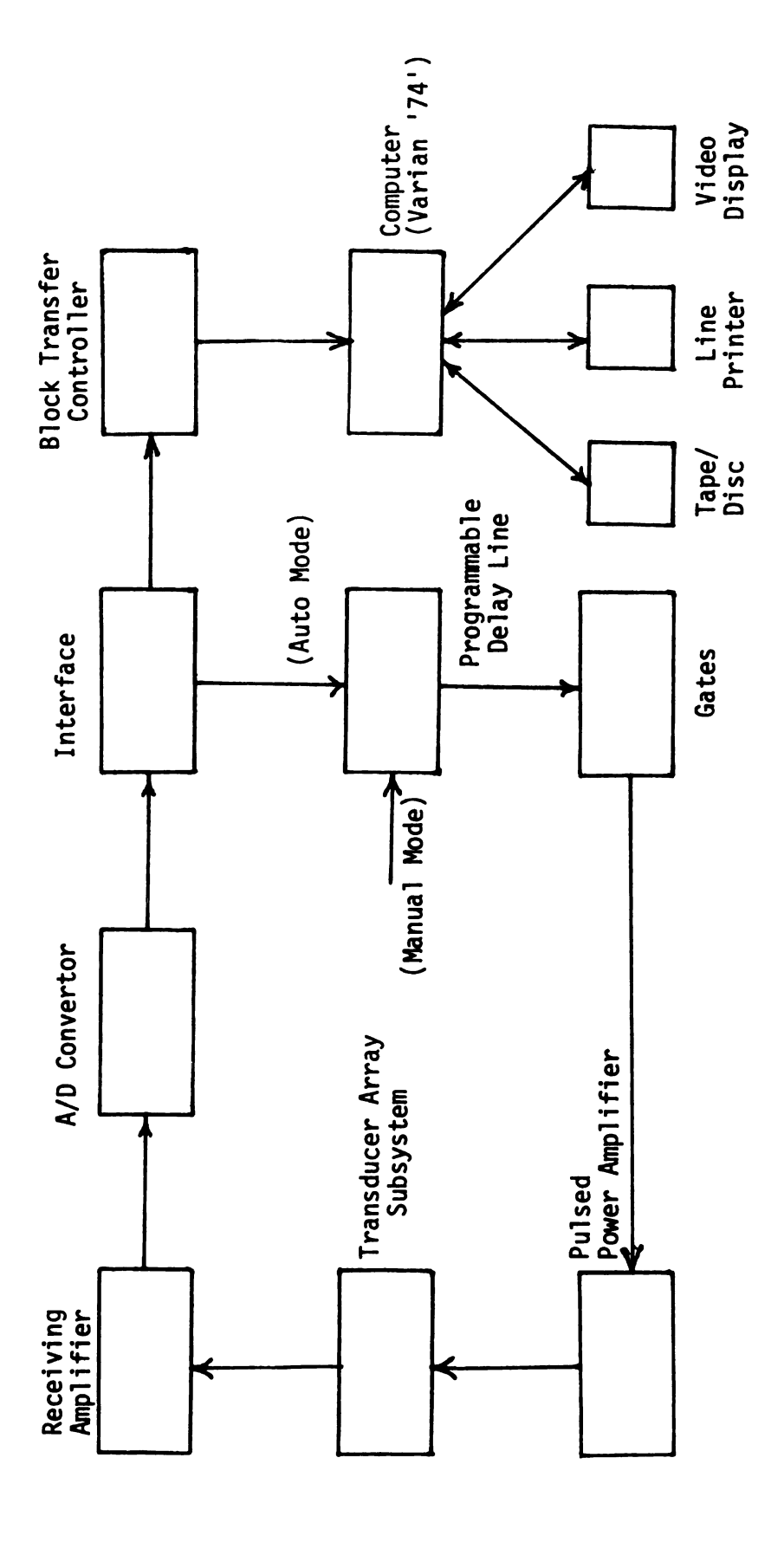


Figure 1 System Block Diagram

+5 volts

with a standard single element transducer.

- 2) The programmable delay line is used to provide necessary delays for each element of the array to steer or focus the beam. It has two modes of operation; the manual mode can be used to manually control the delays by setting external switches. In the automode the computer interface sends an initiating signal called DECX. Once initiated in any mode the programmable delay lines initiate monostables, which have been designed to generate a pulse of 0.3 microseconds at each rising edge of input from the delay lines. These pulses are passed through the gates. The purpose of gates is to avoid loading of the monostable by the power amplifiers which are connected with the gates. There are ten gates so we can get ten pulses delayed by a time controlled by the programmable delay lines which can also be automatically incremented by subsequent DECX pulses coming from the computer. The ten pulses coming out of ten gates are amplified by ten amplifiers and are applied to each element respectively for exciting the transducer.
- 3) The transducer generates the ultrasound waves in pulses depending upon the excitation pulses. For the time interval when the transducer is not transmitting, it can be used as a receiver because the reflections can be detected by the transducer due to its inverse piezoelectric effect. For example, the central element of the transducer may be used as a receiver.
- 4) The reflected pulses are primarily of 1 MHz frequency and after their detection are applied at the input of an amplifier. The output of the amplifier (panametric 5050 Pulser Receiver) is applied to a Biomation A/D converter which samples it at a rate

of 5 MHz.

- 5) The A/D convertor converts each sample to an 8-bit word and stores these words for 400 microseconds (2048 words) in its own memory. Once this memory is full it gives signal to the block transfer controller (part of the computer) through an interface to start transferring all these words to the computer memory and simultaneously initiates the delay lines to start a new cycle of excitations for the transducer.
- 6) From computer memory these words are transferred to the tape and from the tape to the disc. Then, gray levels are assigned for each word and then the image is displayed on a video monitor.

This thesis is limited to design, fabrication and performance testing of the ultrasonic transducer arrays fabricated for this research and a description of the supporting electronics. A description of the computer software, hardware and interfacing is to be found in Mark Funk's master's degree thesis to be published.

CHAPTER II THEORY OF PHASED ARRAYS

The need for arrays of antennas arose when the microwave engineers wanted to increase the directionality range of their antenna systems. As a solution they connected a number of half or quarter wavelength stubs in parallel. Later on, the need for variable directional antennas lead into the development of phased array antennas, where a certain phase delay was introduced for each element depending upon its location in the array system. As a result of this development, it was possible to electronically steer and focus the beams of radiation from these arrays. The need for ultrasonic phased arrays arose in the analogous fashion and such transducers have been developed in order to steer and focus the beams of ultrasonic radiation. (1)

This chapter deals with the theoretical aspects of the ultrasonic phased arrays which includes the derivation of expressions for the field strength of an array and steering and focusing effects by introducing phase delays in the field strength expression. The second half of this Chapter includes the computer simulations from a simple theoretical model for the transducer which was fabricated and tested in this study.

In order to understand the theory of ultrasonic phased arrays, it is necessary to start the discussion with a brief introduction to the acoustic fields. When the particles of a medium are displaced from their equilibrium position, then, as a result of this action, internal restoring forces arise as a reaction. It is these elastic restoring forces

between the particles, combined with inertia of the particles, which leads to the oscillatory motion of the medium. As a result of this vibration in the medium, traveling waves are generated by the medium which travel out of the generating medium. It is this basic phenomenon which is responsible for the production of acoustic fields. (2)

The materials used for generating acoustic fields are normally classified as piezoelectric materials such as were discussed in Chapter 1. A subset of materials exhibiting strong piezoelectric properties are the ferroelectric materials. Lead zirconate is a good example of such a material and it was used in the research done to fabricate the ultrasonic phased array. (3)

Since the piezoelectric materials are anisotropic, the equations relating the electrical to mechanical properties will necessarily involve a large number of coefficients. The six basic coefficients involved in these equations are elastic stiffness coefficient 'c', absolute permittivity 'e', two piezoelectric strain coefficients 'g' and 'd' and two piezoelectric stress coefficients 'e' and 'h'.

Strictly speaking, the equations for a piezoelectric material should be written in terms of tensor notation. (4) However, in order to simplify matters, we assume that when a field is applied parallel to one of the axis the stress or strain will also be in the same direction. Under this assumption the four basic equations relating two electrical quantities, displacement 'D' and field strength 'E' to two mechanical quantities, strain 'S' and tension 'T', describing the direct piezoelectric effect are as follows: (i) $D = \epsilon^T E + dT$

(ii)
$$D = \varepsilon^S E + eS$$

(iii)
$$E = (1/\epsilon^T)D - qT$$

(iv)
$$E = (1/\epsilon^S)D - hS$$
, where

- d = Strain developed/Applied force
- e = Stress developed/Applied force
- g = Strain developed/Applied charge density
- h = Stress developed/Applied charge density
- ε = Dielectric constant

These types of basic equations can be used to derive important results like the field strength expression for one radiating element of an array of ultrasonic antenna. (4)

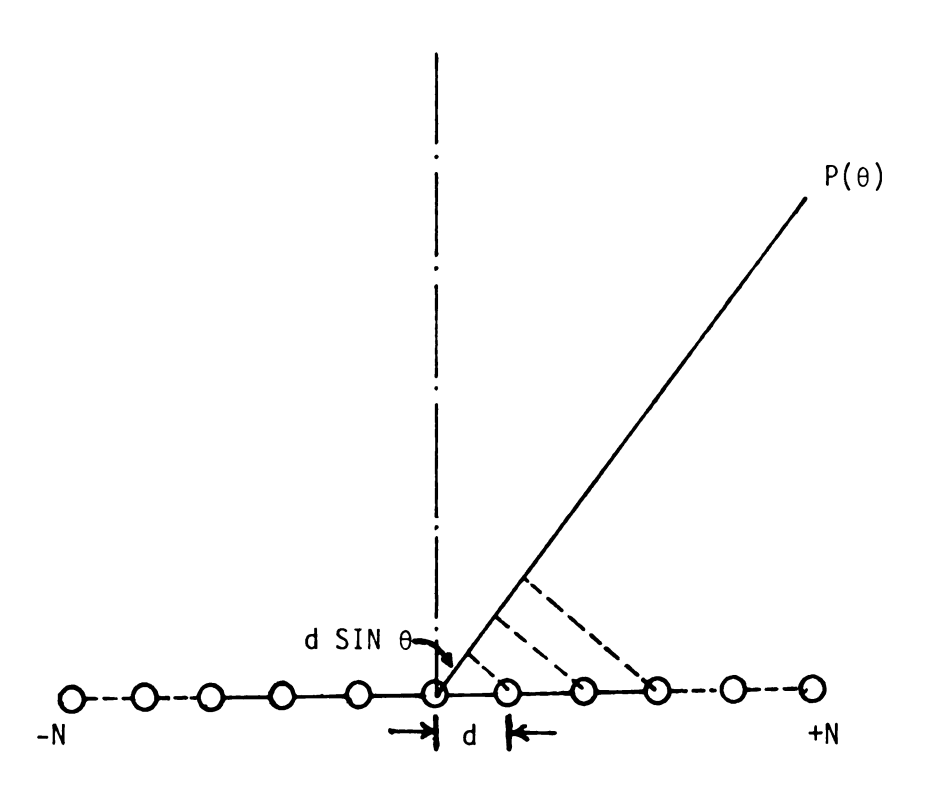
2.1 Field Strength Expression for an Array

This section describes a simplified expression for the acoustic field strength pattern of an array of radiating elements. The first analysis is based on an approximation which holds considerably well for far zones of the field (5) and point source elements. Later sections of the Chapter discuss the field strength expressions for elements of finite dimensions. Theoretical consideration of cross coupling is treated later in this thesis.

The radiation pattern produced by an array of radiating elements will first be derived by considering each element as a radiating point source separated by the same distance as in the actual array fabricated. Then, the overall radiation pattern is the superposition of field patterns produced by all these elements and the patterns produced by all their point sources.

Referring to Figure 2, note that each element is shown as a point source separated by distance 'd' and ' θ ' is the angle of observation of the resultant field strength P(θ).

In the far zone approximation, we approximate the path difference between any two elements or point sources as $d SIN(\theta)$.



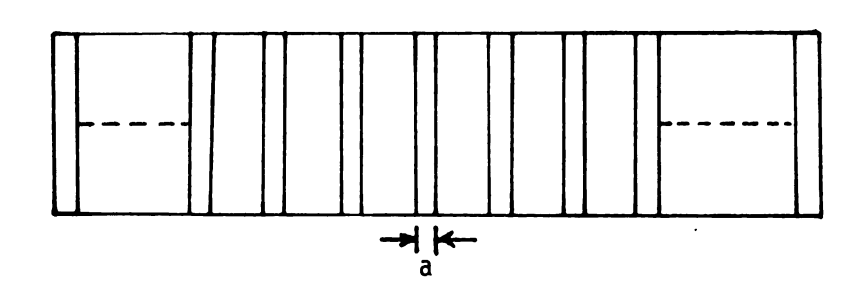


Figure 2 Geometrical Details of an Array

So, the phase difference (u) =
$$\frac{2(\pi)(\text{path difference})}{\text{wave length}}$$

u = $\frac{2(\pi)(\text{d SIN}(\theta))}{\lambda}$

We define P(o) as the acoustic field strength amplitude of each radiating element.

When all point sources (elements) are radiating with no relative time delays, the total field strength for an odd number of elements in an array is given as

5)
$$P(\theta) = P(0) (e^{-iNu} + e^{-i(N-1)u} + ... + 1 + ... + e^{i(N-1)u} + e^{iNu})$$

where 'n' is the actual number of radiating elements; n = 2N + 1

Equation 5 is a geometrical progression and can be simplified as

$$P(\theta) = P(o) (e^{-iNu}(1 + e^{iu} + ... + e^{i2Nu}))$$

$$= P(o) (e^{-iNu}(e^{i(2N + 1)u} - i)/(e^{iu} - 1))$$

$$= P(o) (e^{-i(2N + 1)u/2}(e^{i(2N + 1)U/2} - e^{-i(2N + 1)U/2}))$$

$$= e^{iU/2}(e^{iU/2} - e^{-iU/2})$$

which may be written as

6)
$$P(\theta) = P(0) SIN((2N + 1) U/2)/SIN (U/2)....(1)$$

for an even number of elements in the array, if the field strength is calculated at 3d from the center.

$$P(\theta) = P(0) (e^{-iNu} + e^{-i(N-1)u} + ... + 1 + ... + e^{i(N-2)u} + e^{i(N-1)u})$$

where n the actual number of radiating elements; n = 2N.

The preceding expression is a geometric progression and can be simplified as $P(\theta) = P(o) \ (e^{-iNu}(e^{i2Nu} - I/e^{iu} - 1))$ simplifying

=
$$P(o) e^{-iNu}e^{iNu}e^{iu/2}((e^{iNu}-e^{-iNu})/2i/(e^{iu/2})/2i)$$

= $P(o) e^{-iu/2}(SIN Nu/SIN u/2)$.

So, the magnitude of the expression $P(\theta)$ is given as

7)
$$|P(\theta)| = P(o)$$
 (SIN Nu/SIN u/2)

The expression for a single radiating element of an array antenna is derived from the fundamental equations of the acoustic fields as mentioned in the introduction of the Chapter⁽⁴⁾ and the result is stated below.

The pattern from a single element from finte width 'a' is

8) P(o) = SIN(u')/u'....

where
$$u' = Phi * a * SIN(\theta)/\lambda$$

where 'a' is the width of radiating element, refer to Figure 1. So, the overall expression for the field strength become for 'n' even elements; n = 2N

9A) $|P(\theta)| = A_0(SIN(u')/u') * SIN(Nu)/SIN(u/2)$ (Refer to Equations 7, 8) and for 'n' odd elements

9B)
$$P(\theta) = (SIN(u')/u') * SIN((2N + 1)u/2)/SIN(u/2)$$

(Refer to Equations 6, 8)

These expressions are an approximation for far field strength patterns in which cross coupling is neglected.

Using the above expressions, two computer calculations were performed for plotting the field strength pattern of an array with seven elements and of a single element of the same seven element array. Some of the results are indicated in the following few pages.

Computer Calculation 1

This calculation shows the evaluation of field strength pattern of a seven element array. The data used is as follows:

Spacing between the elements (d) = 1 m.mts

Velocity of ultrasound (V) = 1.5×10^6 m.mts/sec.

Frequency of ultrasound (f) = 10^6 Hz

Width of each array element (a) = 0.4 m.mts

Table 1 Computer Simulation of Field Strength Pattern of an Array

******	Theta (θ) (degrees)	Field Strength P (θ) (dBs)
1)	-45	-19.22
2)	-40	-50.22
3)	-35	-18.04
4)	-30	-17.16
5)	-25	-36.05
6)	-20	-13.77
7)	-15	-15.55
8)	-10	-12.97
9)	- 5	- 2.46
10)	0	0
11)	5	- 2.46
12)	10	-12.97
13)	15	-15.55
14)	20	-13.77
15)	25	-36.05
16)	30	-17.16
17)	35	-18.04
18)	40	-50.22
19)	45	-19.22

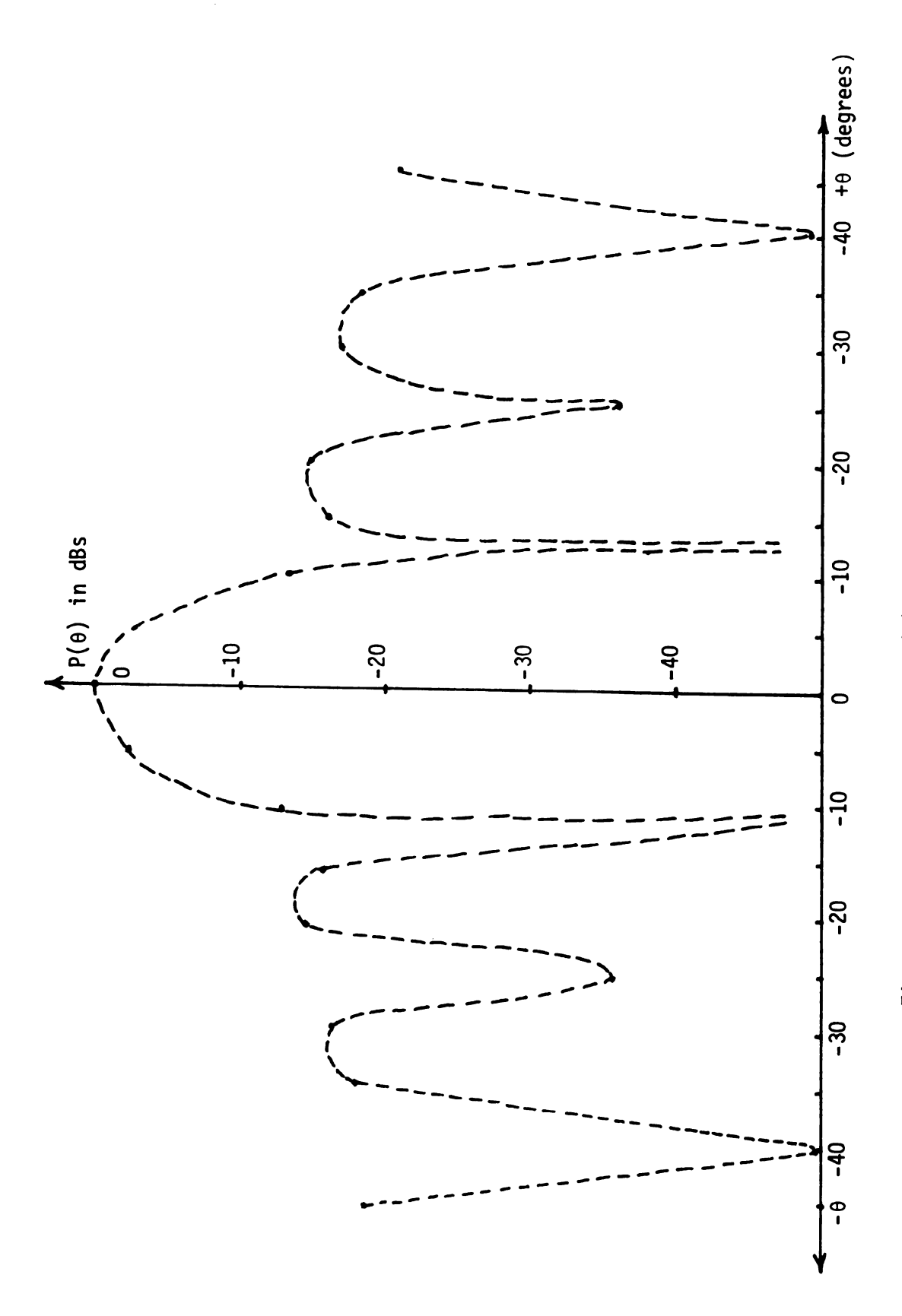


Figure 3 Simulation Plot of $P(\theta)$ vs θ for an Array

Computer Calculation 2

This calculation shows the evaluation of field strength pattern of a single element of a seven element array. The data used is as follows:

Spacing between the elements (d) = 1 m.mts

Velocity of ultrasound (V) = 1.5×10^6 m.mts/sec.

Frequency of ultrasound (f) = 10^6 Hz

Width of each array element (a) = 0.4 m.mts

The following table shows the variation of field strength (in dBs) versus Theta (θ) in the range ± 45 degrees obtained by using the Computer Program 1, Appendix C.

Table 2 Computer Simulation of Field Strength Pattern of an Array Element

	Theta (θ) (degrees)	Field Strength P (θ) (dBs)	
1)	-45	-6.48	
2)	-40	-5.22	
3)	-35	-4.10	
4)	-30	-3.22	
5)	-25	-2.62	
6)	-20	-2.13	
7)	-15	-1.50	
8)	-10	-0.95	
9)	- 5	-0.52	
10)	0	0	
11)	5	-0.52	
12)	10	-0.95	
13)	15	-1.51	
14)	20	-2.13	
15)	25	-2.62	
16)	30	-3.22	
17)	35	-4.11	
18)	40	-5.22	
19)	45	-6.48	

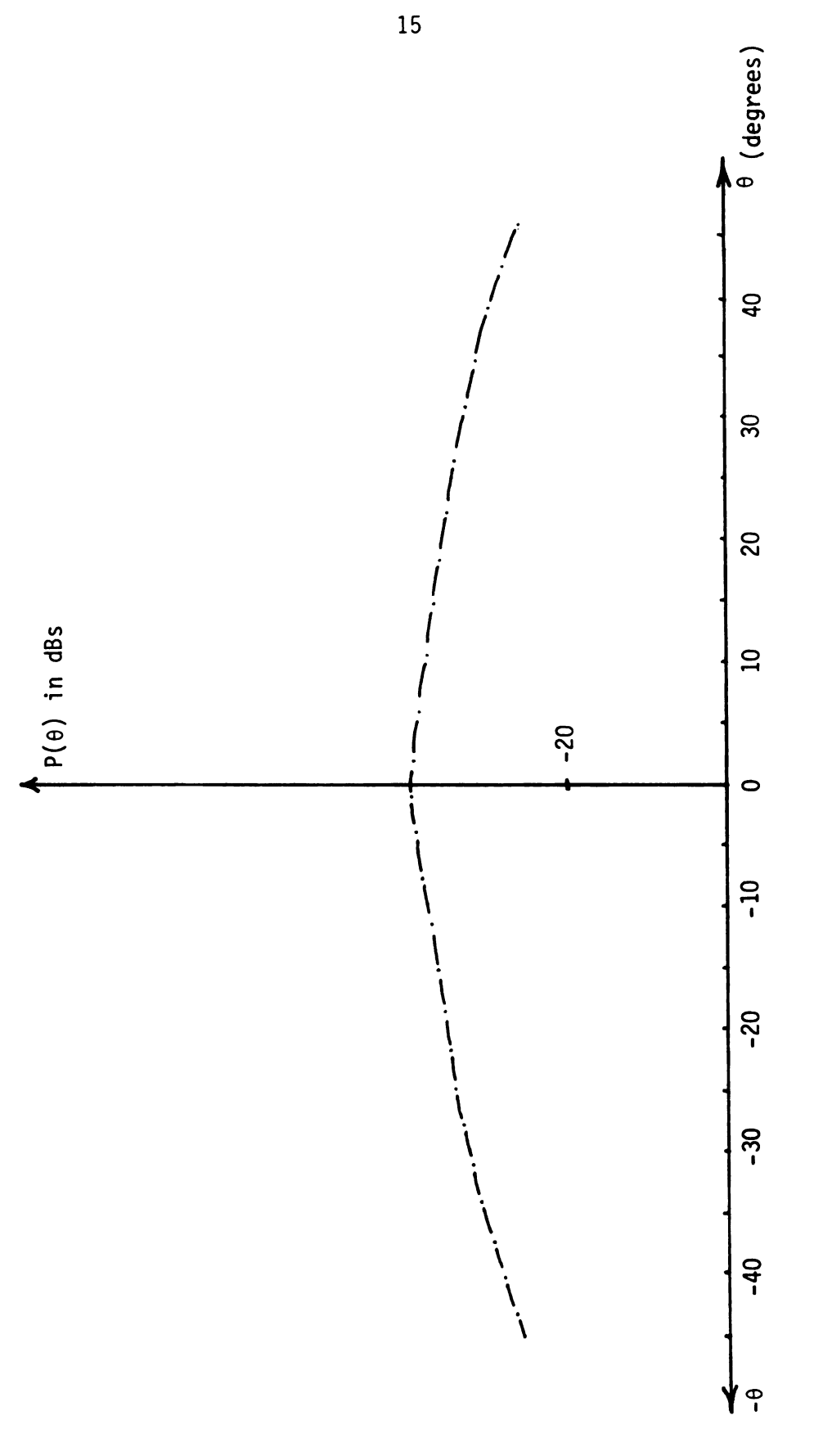


Figure 4 Simulation Plot of $P(\theta)$ vs θ of an Array Element

2.2 Beam Steering

In order to steer the ultrasonic radiation beam being generated by the ultrasonic transducer, one needs to provide appropriate delays to the excitation pulse for each element. (5) This delay depends upon two factors, first, the amount of steering one wants to provide, i.e. the amount by which one wants to shift the central lobe of radiation, and, second, the physical location of the element within the array. For example, suppose one wants to shift the central lobe to the right, then the last element starting the count of elements from left would get the maximum phase shift or time delay. Primarily, the delays are provided so that all radiations reach a particular preselected point at the same time to provide a constructive interference, so that one can get the maximum intensity of the ultrasonic beam. In order to steer the beam for checking the properties of the transducer through small angles like ±5 degrees, one may use a fixed delay line, which are simply lumped models of a transmission line. (See Appendix A for the details of the fixed delay lines used in this study.) For controlling the beam steering electronically through a range up to ±45 degrees, one needs programmable delay lines or phase shifters (see Appendix A for a description of the programmable delay lines used in this study). In order to obtain computational results for beam steering, we can simply subtract an element phase shift due to a time delay from 'u' in the expression (9A) and (9B) of Section 1, resulting in the following expressions for 'n' even numbers.

10) $|P(\theta)| = (SIN (u')/u') * SIN N(u - 2\pi ft)/SIN (u - 2\pi ft)/2$ where f = frequency of radiations

t = time delay required between adjacent elements

 $2\pi ft$ = phase delay of firing and, similarly, for 'n' odd elements

11) $P(\theta) = SIN(u')/u' * SIN ((2N + 1)(u - 2\pi ft)/SIN (u - 2\pi ft)/2)$ Using Expressions (10) and (11) a computer calculation was performed; some of the results are indicated in the following few pages.

Computer Calculation 3

This calculation shows the field strength pattern of a seven element array with a time delay of firing of 0.3 microseconds between consecutive elements to steer the central lobe of the ultrasonic beam by 30 degrees.

The data used is as follows:

Spacing of elements (d) = 1 m.mts

Velocity of ultrasound (v) = 1.5×10^6 m.mts/sec.

Frequency of ultrasound (f) = 10^6 Hz

Width of one array element (a) = 0.4 m.mts

Delay time of firing between adjacent elements (t) = 0.3 μ seconds The following Table shows the variation of field strength (in dBs) versus angle Theta (θ) in the range ± 45 degrees, obtained by using the Computer Program 1, Appendix C.

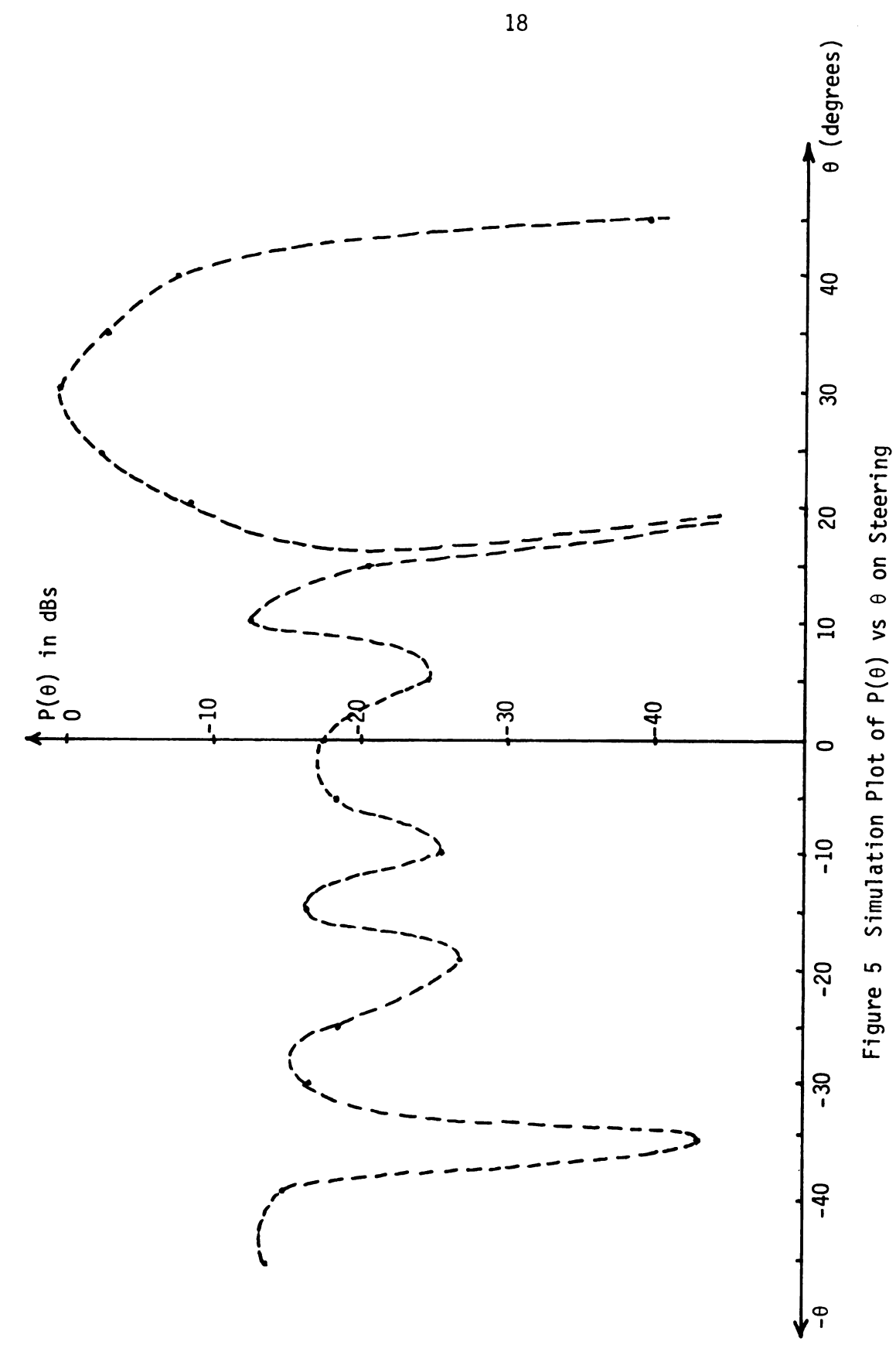


Table 3 Computer Simulation of Field Strength Pattern on Steering

	Theta (θ) (degrees)	Field Strength P (θ) (dBs)	
1)	-45	-13.27	
2)	-40	-15.73	
3)	-35	-42.71	
4)	-30	-16.87	
5)	-25	-18.75	
6)	-20	-27.60	
7)	-15	-16.98	
8)	-10	-25.46	
9)	- 5	-18.55	
10)	0	-17.25	
11)	5	-24.94	
12)	10	-12.83	
13)	15	-20.52	
14)	20	- 9.12	
15)	25	- 1.85	
16)	30	- 0.26	
17)	35	- 2.31	
18)	40	- 8.64	
19)	45	-39.99	

2.3 Beam Focusing

In order to focus the ultrasonic radiation beam being generated by an ultrasonic transducer one needs to provide appropriate delays to the excitation pulse for each element as was necessary for beam steering, the only difference being that the delays required for focusing primarily depend upon the location of the element within an array⁽⁷⁾ and depth of desired focusing. Simple focus requirements reveal the details. Consider a 5-element array focused at depth r on the central axis, as shown in Figure 6. In order to focus the beam what we physically mean is to

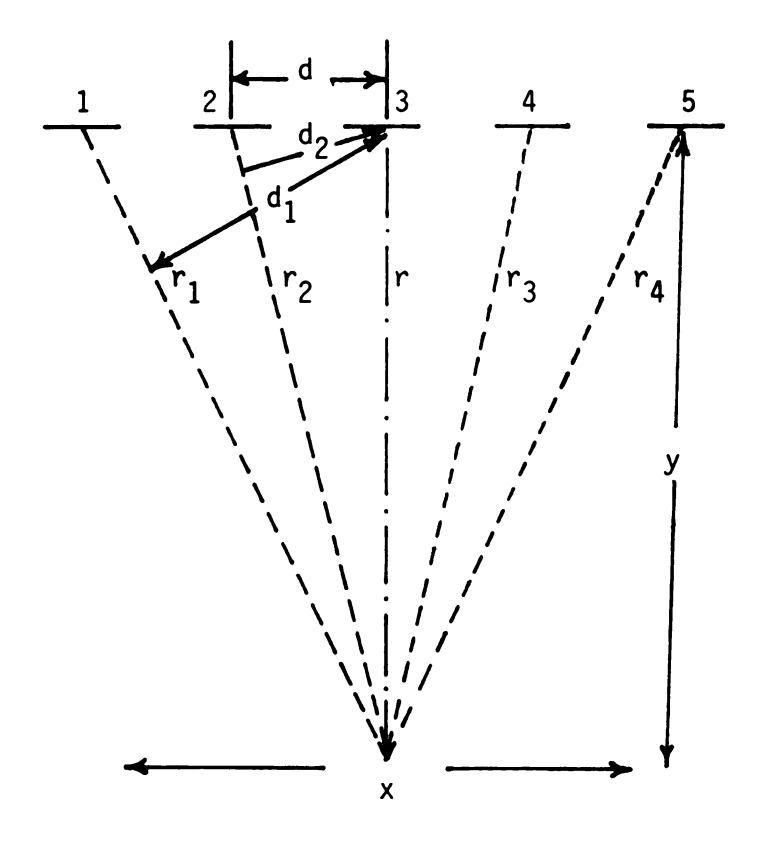


Figure 6 Focusing Effect

produce a constructive interference at the focus point. We can accomplish this by adjusting the phase delays in such a way that the crests of radiations generated by all the elements reach the focus point at the same time. This would mean that as the distance of No. 1 is maximum from the focal point it needs the minimum delay and two needs more delay than 1 and so on; the last element 5 would need the same phase delay as No. 1 and so on. The method for finding the phase delays necessary for each element are discussed in later parts of this section. A mathematical analysis of such a situation is necessary for computer simulation and is described below.

The pressure of spherical ultrasound waves at any observation is given as $= e^{ikr}/r$

where $k = 2\pi/\lambda$; λ being the wave length

r = distance of point of observation from the source

If we introduce a phase delay, as would be necessary for focusing, then the pressure is $= e^{i(D = 2\pi i * r/\lambda)}$

where D represents the phase delay introduced.

The distances r_1 , r_2 , r_3 , r_4 are given as

$$r = \sqrt{(x^2 + y^2)}$$

$$r_1 = \sqrt{((x - 2d)^2 + y^2)}$$

$$r_2 = \sqrt{((x - d)^2 + y^2)}$$

$$r_3 = \sqrt{((x + d)^2 + y^2)}$$

$$r_{\mu} = \sqrt{((x + 2d)^2 + y^2)}$$

So, the pressure is given as

12)
$$P(x,y,z) = |(e^{i(D_1 + 2 \cdot \pi (r_1 - r)/\lambda)/ri} + e^{i((D_2 + 2 \cdot \pi (r_2 - r)/\lambda/r_2))} + e^{i(D_3)/r_3} + e^{i((D_4 + 2 \cdot \pi (r_3 - r)/\lambda))/r_4} + e^{i((D_5 + 2 \cdot \pi (r_4 - r)/\lambda)/r_5)})|$$

where the r_i are taken to be equal in the denominators. In order to find

the values of phase delays; D's refer to Figure 6.

$$d_1 = (2 * d) SIN(Arc TAN(2 * d/z)) = d_5$$

$$d_2 = (1 * d) SIN(Arc TAN(1 * d/Z)) = d_4$$

where Z is the third coordinate value of the location of the focus point along the z-axis so,

 $t_1 = t_5 = d_1/Velocity$ of ultrasound waves in the medium

 $t_2 = t_4 = d_2/Velocity$ of ultrasound waves in the medium

where t_1 , t_2 , t_4 , t_5 describes the time delay of firing for elements

1, 2, 4, 5, respectively, so

13A)
$$D_1 = D_5 = 2 * \pi * f * t_1$$

13B)
$$D_2 = D_4 = 2 * \pi * f * t_2$$

where D_1 , D_2 , D_4 , D_5 represents phase delays for respective elements, where f is the frequency of ultrasound waves and the velocity of ultrasound waves in water is about 1,500 meters per second.

Using Expressions 12 and 13, a computer simulation for focusing was done and some of the results are listed below.

Computer Calculation 4

This calculation shows the effect of focusing on the field strength pattern. The data used is as follows:

Spacing between elements (d) = 1 m.mts

Depth of measurement (y) = 100 m.mts

Focal point or beam focusing point (z) = 100 m.mts

Velocity of ultrasound (v) = 1.5×10^6 m.mts/sec.

Frequency of ultrasound (f) = 10^6 Hz

The following Table shows the variation of field strength (dBs) versus the x - axis variation keeping the y and z axis dimensions constant; obtained by using Computer Program 2, Appendix C.

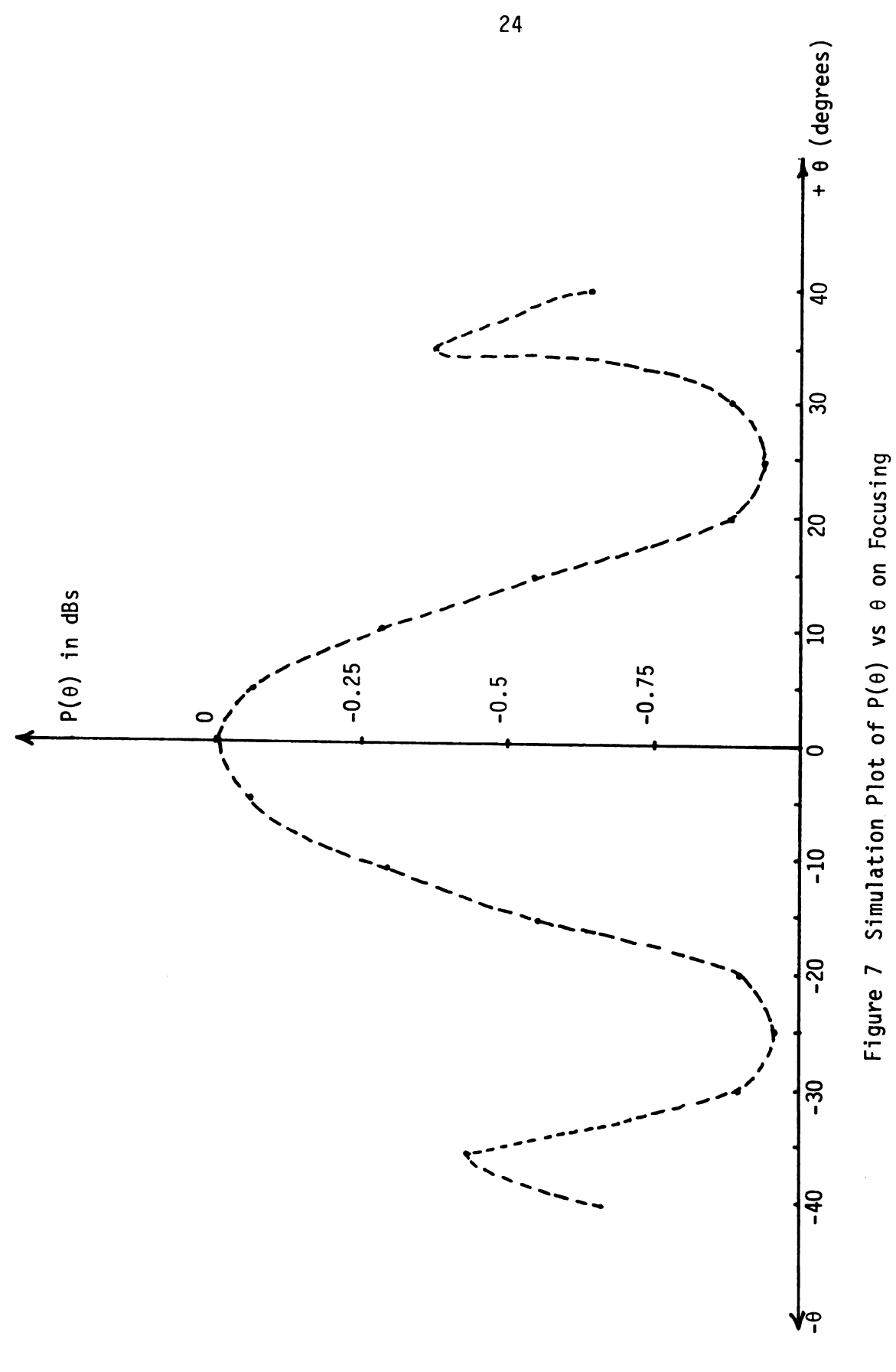
Table 4 Computer Simulation of Field Strength Pattern on Focusing

	Axial Distance (x) (m.mts)	Field Strength P (θ) (dBs)
1)	-40	-0.65
2)	-35	-0.34
3)	-30	-0.81
4)	-25	-0.93
5)	- 20	-0.80
6)	-1 5	-0.56
7)	-10	-0.28
8)	- 5	-0.08
9)	0	-0.00002
10)	5	-0.08
11)	10	-0.28
12)	15	-0.55
13)	20	-0.80
14)	25	-0.92
15)	30	-0.80
16)	35	-0.33
17)	40	-0.65

2.4 Expressions for a Circular Element Transducer

When the individual elements of an array cannot be modeled as point sources or as infinite lines of finite width, the analysis becomes more difficult. The basic technique involved in these complicated derivations is that one has to integrate over the surface of the radiator assuming each surface element dS acts as a spherical radiator. (8) As a result of this integration, the expressions which are formed are given below. Here the results for a finite circular element are considered.

In the far field where the patch difference can be approximated by d SIN(θ) where d is the spacing between elements and θ is the angle of observation.



Furthermore, the distance r of observation from the transducer is assumed much larger than 'a' the diameter of the piston type transducer. This approximation basically separates the near zone and far zones of observation.

The pressure distribution may be found to be given by (Reference 7B)

14)
$$P = \rho * c * k * \pi * a^2 V (2J_1 (k * a * SIN(\theta)) / (2(\pi)r * k * a * SIN(\theta))$$

 ρ = Density of the medium

c = Propagation velocity

k = Wave Constant

V = Velocity amplitude of source

 J_1 = Bessels Function

And the intensity is defined as $I = P^2/2 * \rho * c$

In the 'NEAR ZONE' (8) where the point of observation is of a distance which is comparable to the diameter of the piston transducer and path difference = $d SIN(\theta)$ does not hold so (7B)

$$P = Re (P(o)(e^{2i * \pi * R (-N)/\lambda/R(-N)} + ... + e^{2i * \pi * R(n)/\lambda/R(N)})$$

where R(N) is simply a notational symbol being given as

15)
$$R(N) = (r^2 + N^2d^2) SQRT. - r$$

N being the element number

d being the separation between elements

r is the distance of observation from the axis of the transducer vertically downwards

 λ is the wave length of ultrasonics

2.5 Expressions for a Rectangular Elements Array

Here the source pattern is described as a function of x and y coordinate positions rather than θ as shown in Section One.

Let x_0 , y_0 be the position of the point where the source field pattern is being measured and 'B' indicates the appropriate phase shift provided to each element in comparison to the last element. So, the source field pattern for the far field is given as $^{(5)}$

 $P(x_0, y_0) = e^{jkz} e^{jkr_0^2/2z} (x SINC (\frac{x_0x}{\lambda z}) * S comb (sx_0w/\lambda z) SINC (x_0w/\lambda z)) * y SINC (y_0y/\lambda z)$

 λ = Lambda, Wave Length

n = Number of Elements in the Array

where s comb $(sx_0/\lambda z)$ = Sum all terms $\delta (x_0/\lambda z - n/s)$

 $k = 2 \pi/\lambda$

All other terms are referred to Figure 8.

In a similar way focusing field source patterns may be analyzed as well. (5)

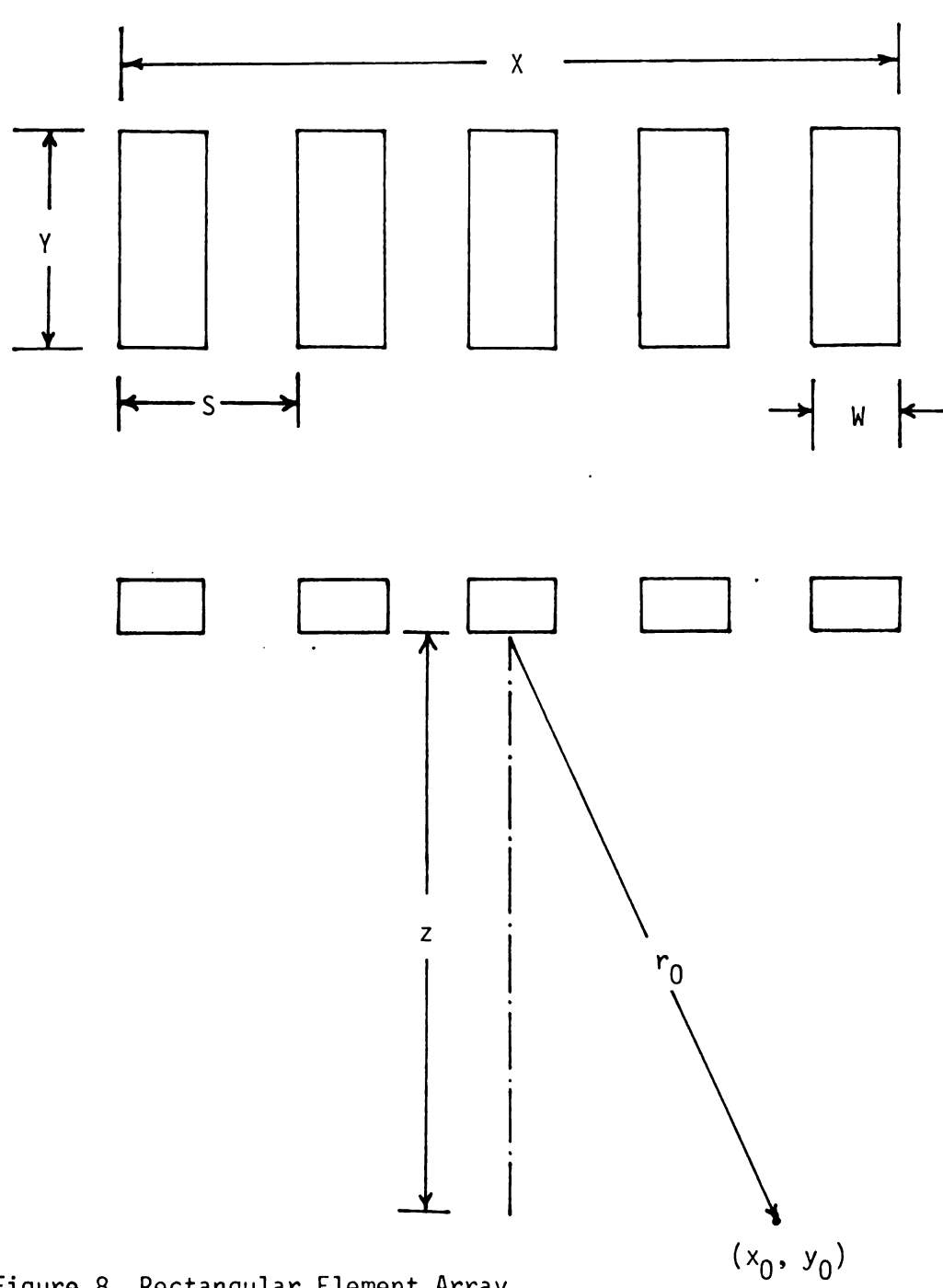


Figure 8 Rectangular Element Array

CHAPTER III ULTRASONIC PHASED ARRAY FABRICATION

This chapter deals with the fabrication technique developed during the course of this research project. The details of fabrication are mentioned below in a stepwise order as follows:

1) Normally the piezoelectric materials are available in large circular discs with silver top and bottom electrodes, so the first step is to cut the disc in small pieces of required dimensions using a diamond wheel saw; the dimension of the piece depends upon how many elements one has to have in the array and the dimensions of the individual elements. Cutting of the piezoelectrical material is a very delicate process and it involves considerable care with the saw and a special process. Before cutting the piezoelectric disc, it is fastened on the base plate of the saw using Apiezon Wax. This should be done very carefully to avoid exceeding the Curie temperature of the piezoelectric; for lead zirconate, the material used for fabrication of the array, the Curie temperature is 160 to 170 degrees centigrade.

Once the disc is firmly held on the base plate, it is ready for cutting. The width of the diamond blade used in the diamond saw depends upon the dimensions of the array; the blade used has a width of 0.25 mm.

First, cut the large disc in small pieces, in this case, the small rectangular piece has the dimension 1.4 cms by 0.7 cms.

These dimensions were selected in order to accomodate 11 elements in the array.*

2) Mount the base plate carefully on the saw and mark on the vertical control handle of the saw the required depth of each cut. For the array fabricated in this study, it was 3/4 of the total depth of the piece.

Then the saw is started and its autohandle locked. Using the automatic feed, after 5 minutes, the first cut should be complete with a speed setting of "40".

It is important to note that autofeed should not be started until after the saw rotation is started. After the cut is finished, move the blade upwards so that it does not touch the piece of piezoelectric, turn off the automatic feed and then the saw. Now, move the horizontal position control handle by an amount such that the spacing between the first and the second cut is the desired amount, which was 1 mm in this case. Then, lower the blade again to the same position as for the first cut and start the saw and autofeed again. In a similar way 12 cuts are made resulting in an 11 element array each 0.6 mm wide, if the cut to cut separation is 1 mm as shown in the Figure 9. It is to be noted that the speed of the saw, if not properly matched with the elasticity of the material to be cut, can result in breaking of the saw blade. A marked speed of 40 units is normally employed for all cutting.

- 3) Once the cutting was complete, a thin wire (32 ohms/cm) was soldered to each element and then the base plate, to which the
- * Only 7 elements were used in actual testing due to problems with the end elements.

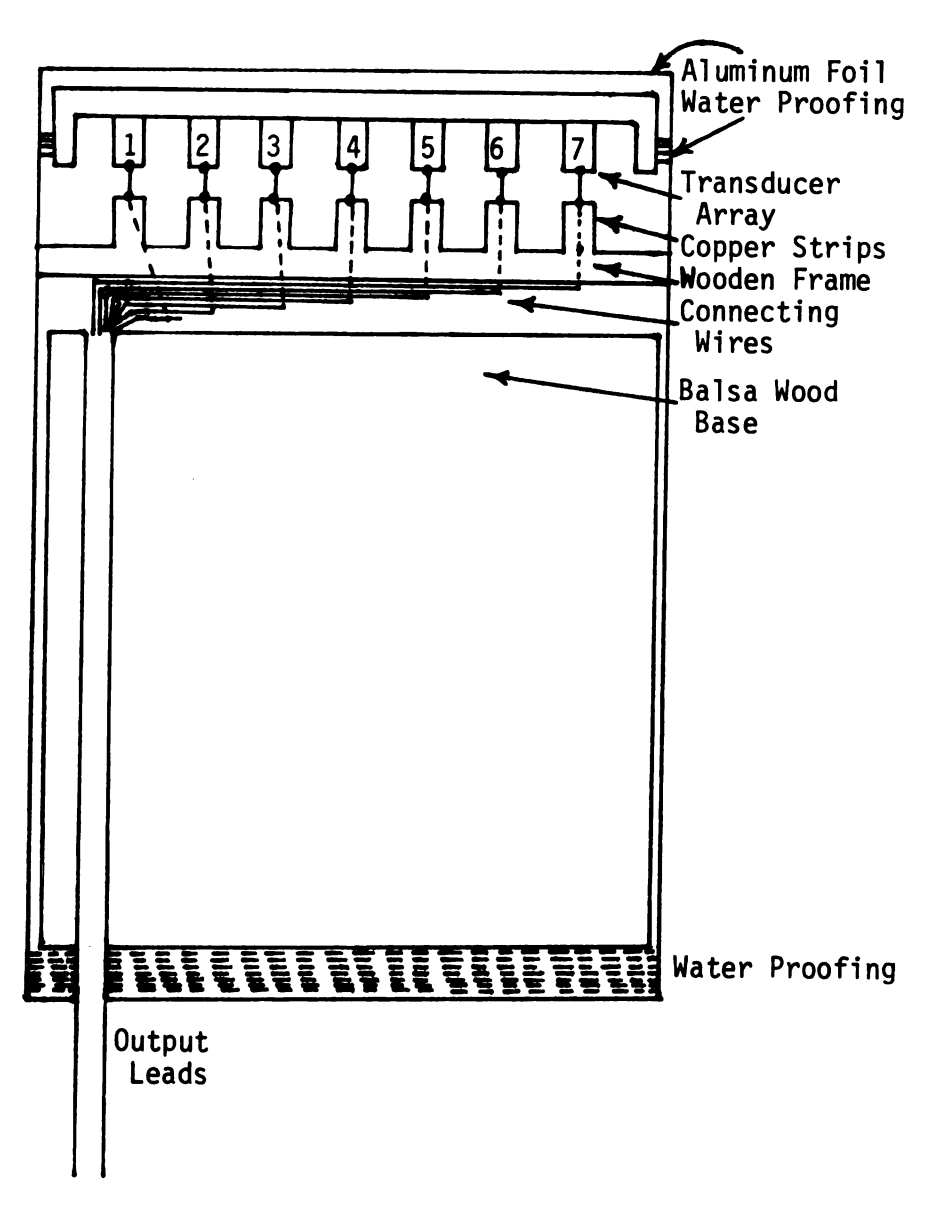


Figure 9 Fabrication Details of Transducer

rectangular piezoelectric piece was glued, was dipped in an acetone filled beaker to remove the wax, in this way the rectangular piece is removed from the base plate and made ready for mounting. 32 ohms/cm thin wire is, infact, not desirable because it causes a certain excitation power drop, but was used as it was the only thin wire available. In the future, wires with such a high resistance should be avoided.

It is worth noting that soldering is the most delicate part of this fabrication technique and should be done very carefully. It is also recommended to use silver solder to make connections in order to increase the strength of the connection.

- 4) A circular balsa wood (insulator) frame was made to fit in a hollow steel cylinderical case as shown in the Figure 9. Then, a rectangular hollow cup was made in its center, with dimensions 1.8 mm by 0.9 mm of depth 3.0 m.mts.
- 5) A damping material was developed in the laboratory by mixing very fine powdered glass with Elmer's Epoxy in a proportion of 2 to 1. This material has the property of damping the ringing oscillations of the elements since its acoustic impedance is higher than balsa wood. Ideally, the damping impedance should be even higher. The compound used represents a compromise between high electrical insulation and high acoustic impedance.
- 6) On the bottom of the balsa wood frame, 11 square pieces of thin copper sheet (0.2 cm by 0.2 cm) were attached using Elmer's Epoxy (Resin and Hardner), each piece completely isolated from the other. These copper pieces were used as a connecting board between the thin wires coming from the transducer elements and the external connecting wires which were to go out of the

assembly.

- 7) When the copper pieces were attached, we filled the rectangular hollow cup in the balsa wood frame with the damping material developed and then mounted the transducer on top, as shown in Figure 9, such that its flat surface was in level with the top surface of the balsa wood frame. This assembly rested for 24 hours so that the damping material dried out.
- 8) Next, connect each of the thin wires coming from each element of the array to each copper piece and also connect the external wires, one with each copper piece.
- 9) Fix the balsa wood frame inside the steel cylinder such that the top surface of the frame is in level with the top side of the cylinderical case. Apply a light coat of silver conducting paint on the top face of the transducer and the edges of the hollow steel case and then attach over the top surface a thin tin foil. Seal the edges of the foil with Elmer's Epoxy to make it waterproof. Fill the bottom of the assembly also with the same water repellant epoxy after connecting a small screw from the outside, to make it waterproof from the bottom also. Attach to the screw a common ground wire for the assembly and solder it to the body of the steel case. This completes the fabrication of the array.

CHAPTER IV EXPERIMENTAL RESULTS

After the fabrication of the transducer, a series of experiments were performed on this transducer in order to check its charaacteristics. The experiments ranged from simply observing the field strength pattern of the array and then checking for the field strength pattern of each element in the array, to the more complex observations of the steering and focusing characteristics of the array.

Some of these results, along with the block diagrams of the controlling electronics, are presented in this chapter. The experiments are divided into two groups and the explanation and observations are stated in the following sections of this Chapter. A discussion of the results presented in this Chapter is in Chapter 6.

4.1 Group 1 Experiments

The Group 1 Experiments consist of the two experiments done to observe the field strength pattern of the array and of the elements individually using a Tone Burst Excitation. The block diagram of the controlling electronics is shown in Figure 10.

In order to generate a tone burst consisting of a 1MHz sinosoidal signal, one needs a pulse generator (Data Pulse Model #106); the output of which can be applied as the trigger input to the tone burst generator (Wave Tek Model #134) operating in gated mode. By adjusting the frequency of the sinosoidal signal of the wave tek generator, one can obtain the desired tone burst. This tone burst is normally of small magnitudes, on

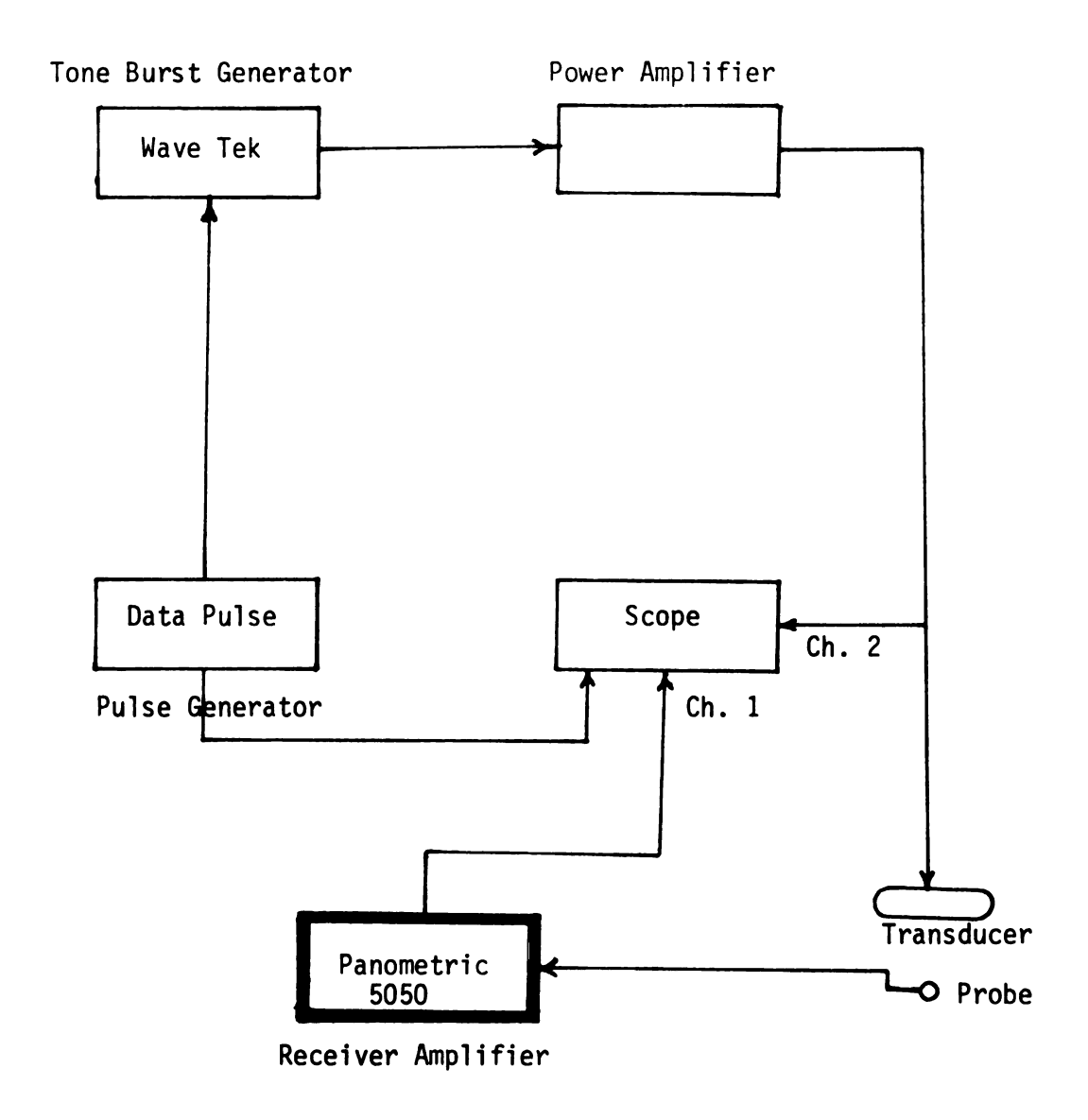


Figure 10 Controlling Electronics of Group 1 Experiments

the order of 1 volts peak to peak which cannot excite the transducer; the transducer needs large voltage for excitation. So, a power amplification is needed and a power amplifier can be connected at the output of the wave tek. From the output of the power amplifier the transducer or the individual elements can be excited. The data obtained in Experiments 1 and 2 is stated below.

Experiment 1

This experiment indicates the variation of field strength of the array, all seven elements excited at the same time versus the axial displacement 'x' about the center of the transducer array. (See Figure 11 for plot.)

Separation between transmitter and receiver = 8 cms

Number of sinosoidal signal cycles in tone burst = 4

Repetition rate of receiving amplifier (panometric 5050) = maximum

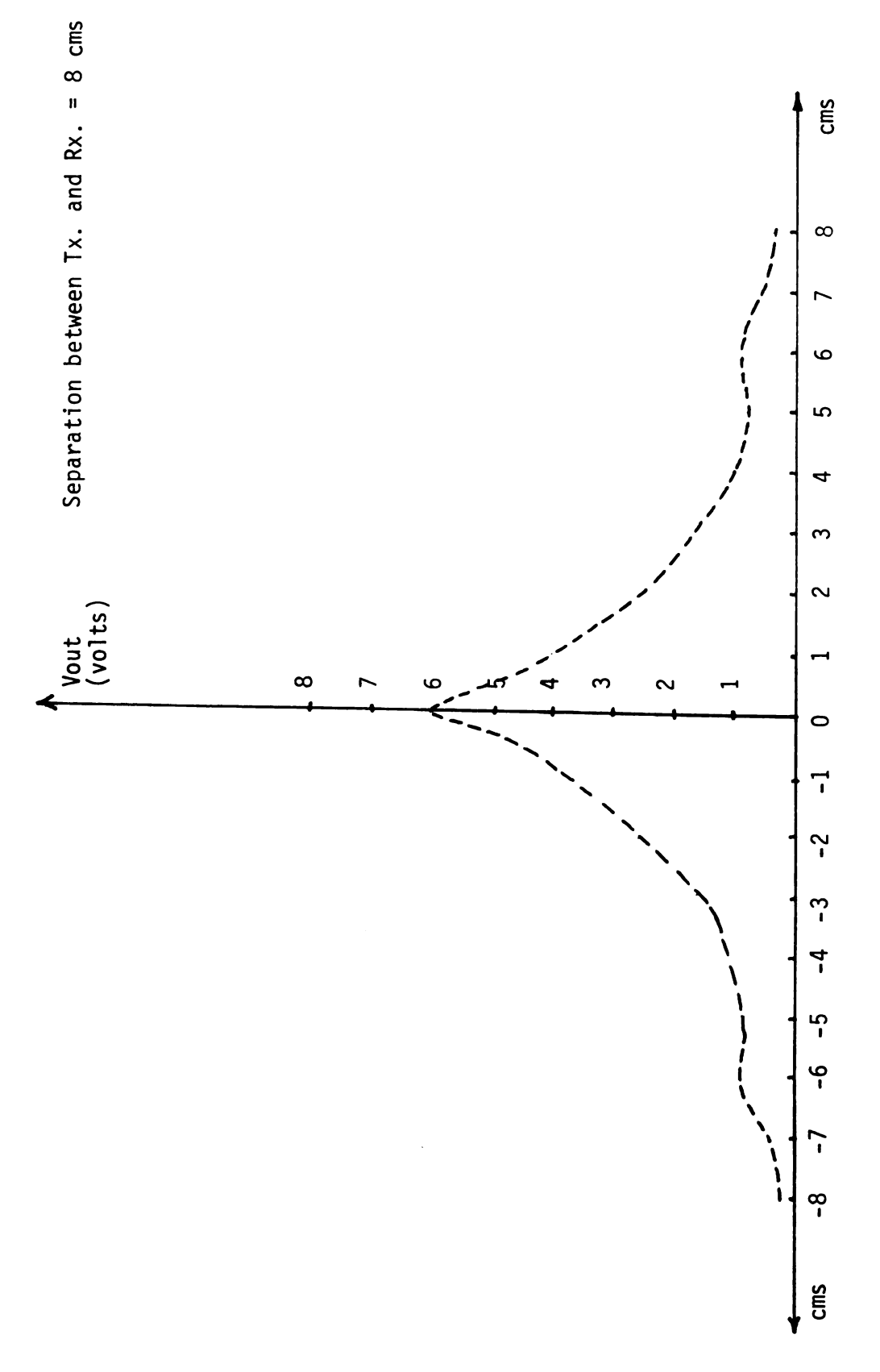


Figure 11 Plot of Vout vs Axial Displacement of an Array

Table 5 Output Voltage versus Axial Displacement of an Array

	Axial Displacement (cms)	Peak to Peak Signal Output (volts)
1)	8	0.30
2)	7	0.51
3)	6	0.95
4)	5	0.80
5)	4	1.00
6)	3	1.80
7)	2	2.50
8)	1	4.00
9)	0	6.00
10)	-1	3.81
11)	-2	2.60
12)	-3	1.70
13)	-4	1.25
14)	-5	0.82
15)	- 6	0.90
16)	-7	0.42
17)	-8	0.35

This Experiment shows the field strength pattern of the central element of the array versus the axial displacement 'x' about the center of the transducer array. (See Figure 12 for plot.)

Separation between transmitter and receiver = 8 cms

Number of sinosoidal signal cycles in tone burst = 4

Repetition rate of receiver amplifier (panometric 5050) = maximum

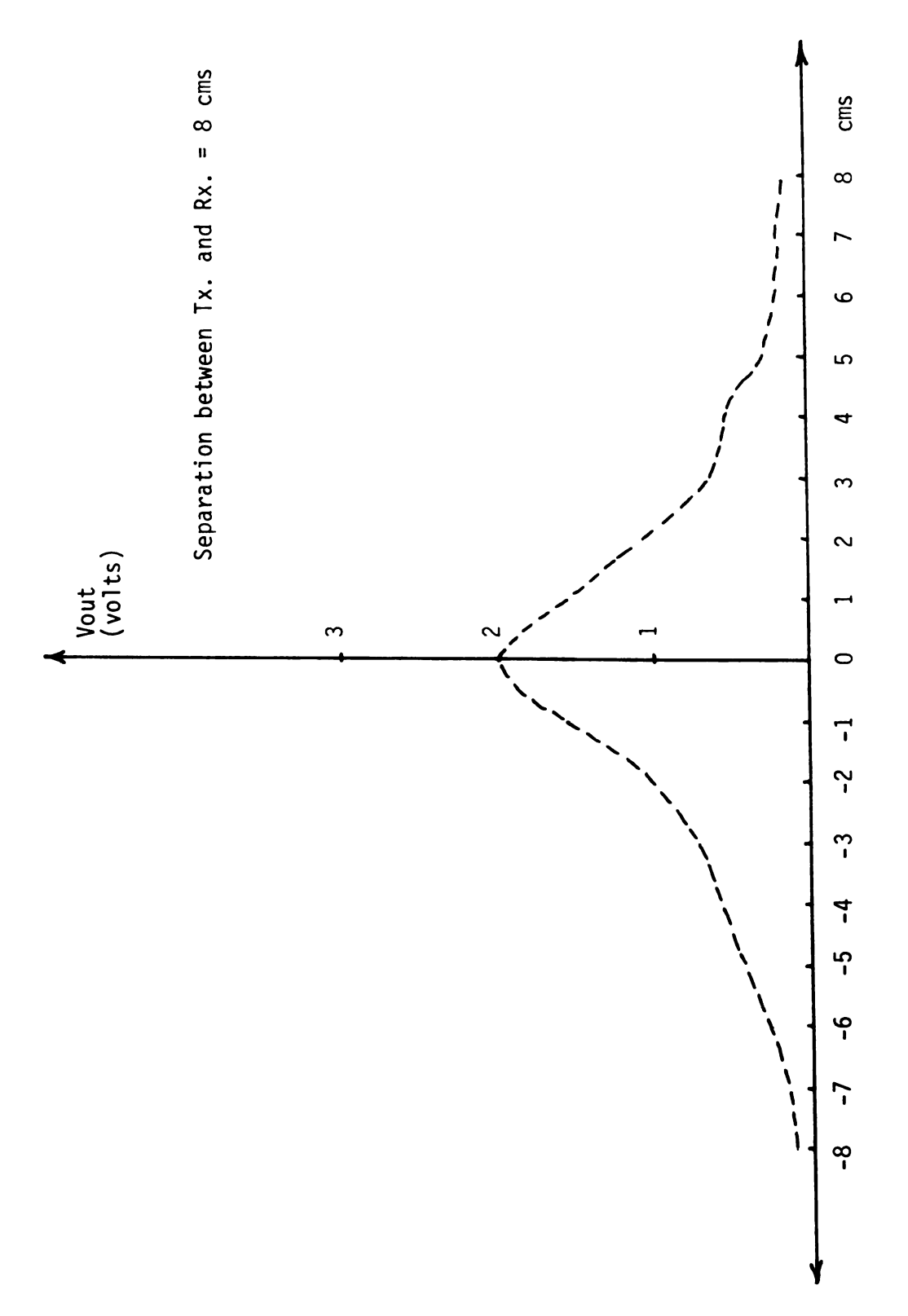


Figure 12 Plot of Vout vs Axial Displacement of an Array Element

Table 6 Output Voltage versus Axial Displacement of an Array Element

	Axial Displacement (cms)	Peak to Peak Signal Output (volts)
1)	8	0.12
2)	7	0.18
3)	6	0.20
4)	5	0.30
5)	4	0.54
6)	3	0.60
7)	2	1.10
8)	1	1.50
9)	0	2.00
10)	-1	1.52
11)	-2	1.00
12)	-3	0.70
13)	-4	0.56
14)	-5	0.40
15)	-6	0.25
16)	- 7	0.15
17)	-8	0.10

4.2 Group 2 Experiments

In this group of experiments, six experiments were performed using an excitation pulse of 0.3 microsecond duration. The last four experiments were performed for steering the beam electronically. For achieving this objective, a programmable delay line network was needed. One such network was developed using digital design techniques during the course of this research. The details of this circuit can be seen in the Appendix A at the end of this thesis. The general block diagram of the supporting electronics is shown in the Figure 13. The programmable delay line gives us ten delayed pulses, the delay between pulses is dependent upon the comparison between the clock rate and the rate at which the DECX

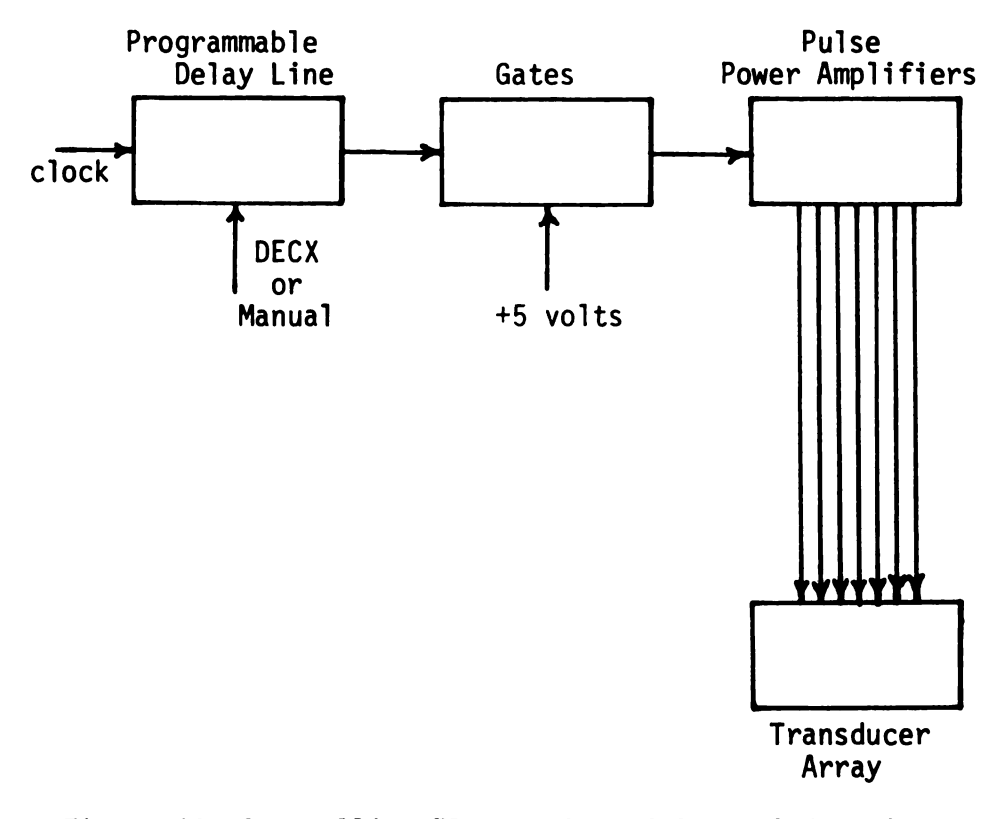


Figure 13 Controlling Electronics of Group 2 Experiments

pulses are coming when operating in auto mode. In the manual mode, as soon as the clock pulse count becomes equal to the preset count reading, we get a pulse which is our output from the programmable delay lines. The change of level of this pulse can be used to trigger a monostable to generate pulses of duration of 0.3 microseconds. These pulses are the input to the power amplifiers (see Appendix B for details) after passing them through the gates. There are ten outputs of the programmable delay line so we need ten gates. The power amplifiers are necessary to provide the high voltage pulses for the excitation of the transducer elements. The delay time between the exciting pulse for each element is controlled by switches attached to the programmable delay line in the manual mode and by the DECX signal (coming from the computer) in the auto mode. This delay time determines the angle through which the main lobe (beam) is steered. It is to be noted that the data obtained during this group of experiments will have some error because one of the seven elements of the array stopped operating during experimentation. The data obtained during the six experiments performed is listed in the following few pages.

Experiment 1

This experiment indicates the field strength pattern of the array with all six elements excited at the same time by a pulse of 0.3 microseconds duration versus the axial displacement 'x' about the center of the transducer array. (See Figure 14 for plot.)

Separation between transmitter and receiver = 7.5 cms

Exciting pulse amplitude = 104 volts

Noise level at the output = 0.03 volts

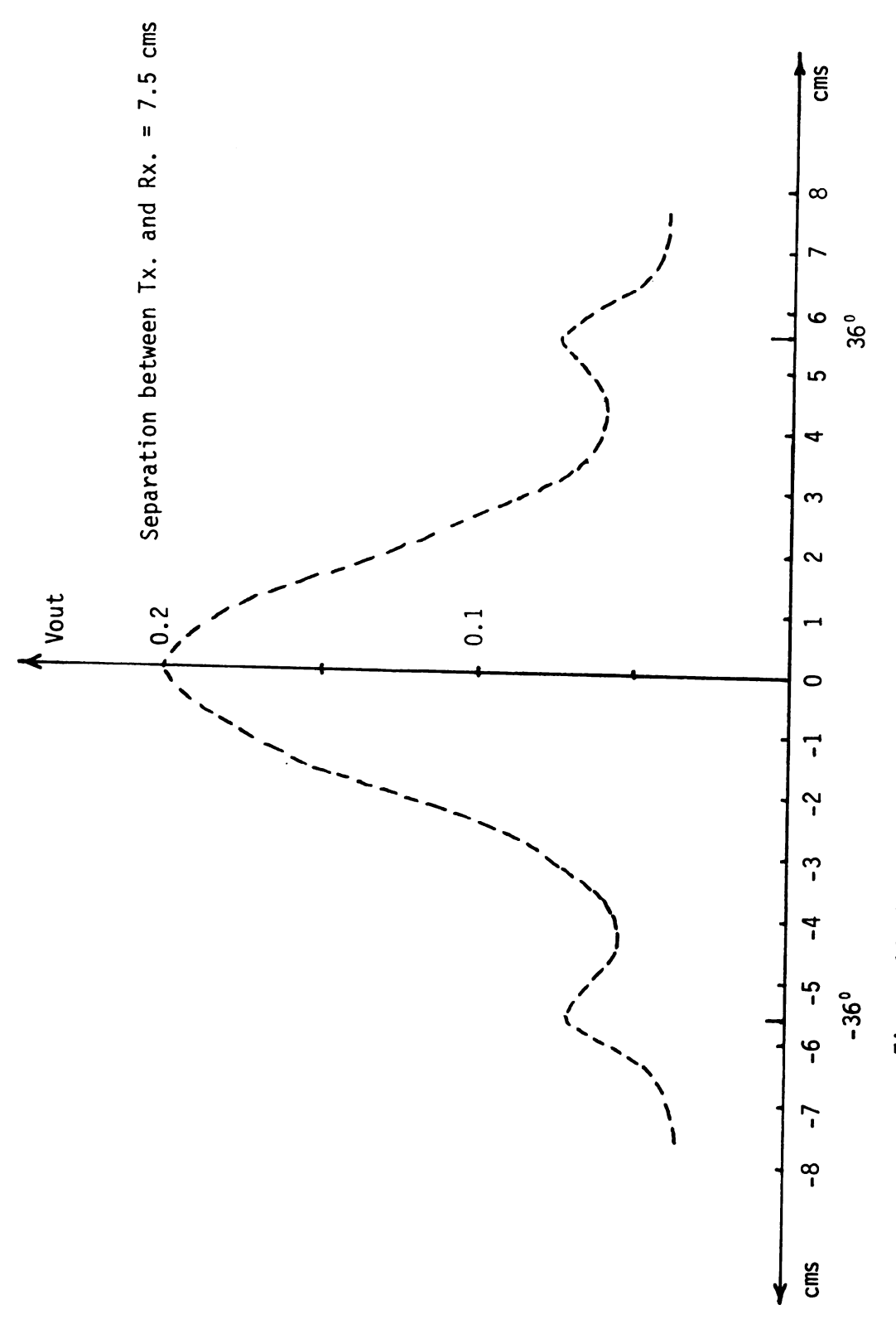


Figure 14 Plot of Vout vs Axial Displacement of an Array

Table 7 Output Voltage versus Axial Displacement of an Array

	Axial Displacement (cms)	Peak to Peak Signal Output (volts)
1)	7.5	0.040
2)	6.5	0.045
3)	5.5	0.074
4)	4.5	0.060
5)	3.5	0.065
6)	2.5	0.100
7)	1.5	0.160
8)	0.5	0.180
9)	0	0.200
10)	-0.5	0.170
11)	-1.5	0.160
12)	-2.5	0.090
13)	-3.5	0.060
14)	-4.5	0.055
15)	-5.5	0.070
16)	-6.5	0.040

This experiment indicates the variation of field strength of the central element alone, excited by a pulse of 0.3 microseconds duration versus the axial displacement 'x' about the center of the transducer array. (See Figure 15 for plot.)

Separation between transmitter and receiver = 7.5 cms

Exciting pulse amplitude = 104 volts

Noise level at the output = 0.03 volts

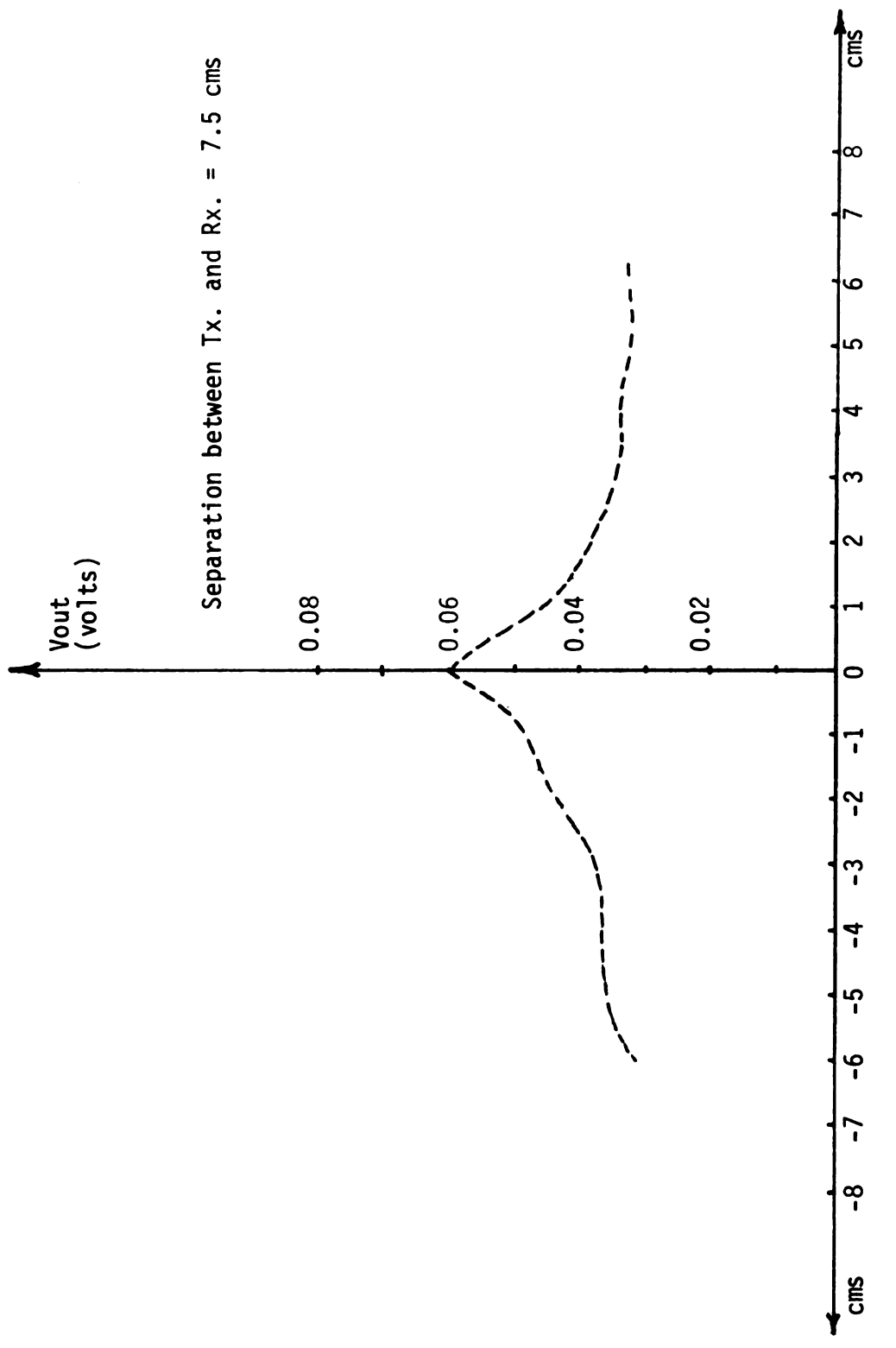


Figure 15 Plot of Vout vs Axial Displacement of an Array Element

Table 8 Output Voltage versus Axial Displacement of an Array Element

	Axial Displacement (cms)	Peak to Peak Signal Output (volts)
1)	5.5	0.031
2)	4.5	0.032
3)	3.5	0.032
4)	2.5	0.035
5)	1.5	0.040
6)	0.5	0.053
7)	0	0.060
8)	-0.5	0.050
9)	-1.5	0.045
10)	-2.5	0.038
11)	-3.5	0.035
12)	-4.5	0.035
13)	-5.5	0.033

This experiment shows the variation of field strength on electronically steering the beam using the programmable delay line. Each of the excitation pulses are of 0.3 microsecond duration. The delay between each of the seven pulses is the deciding factor for the steering angle of the main lobe of ultrasound being transmitted by the array. In order to steer the beam through 30 degrees, one needs a 0.3 microsecond delay between each of the exciting pulses, which, in other words, corresponds to a clock frequency of 3.334 MHz. The programmable delay line designed has the capability of steering the beam towards left or right along the axial displacement axis 'x'. In this particular experiment we want to steer the beam towards left by 30 degrees. The data obtained is as follows: (See Figure 16 for plot.)

Separation between transmitter and receiver = 7.5 cms

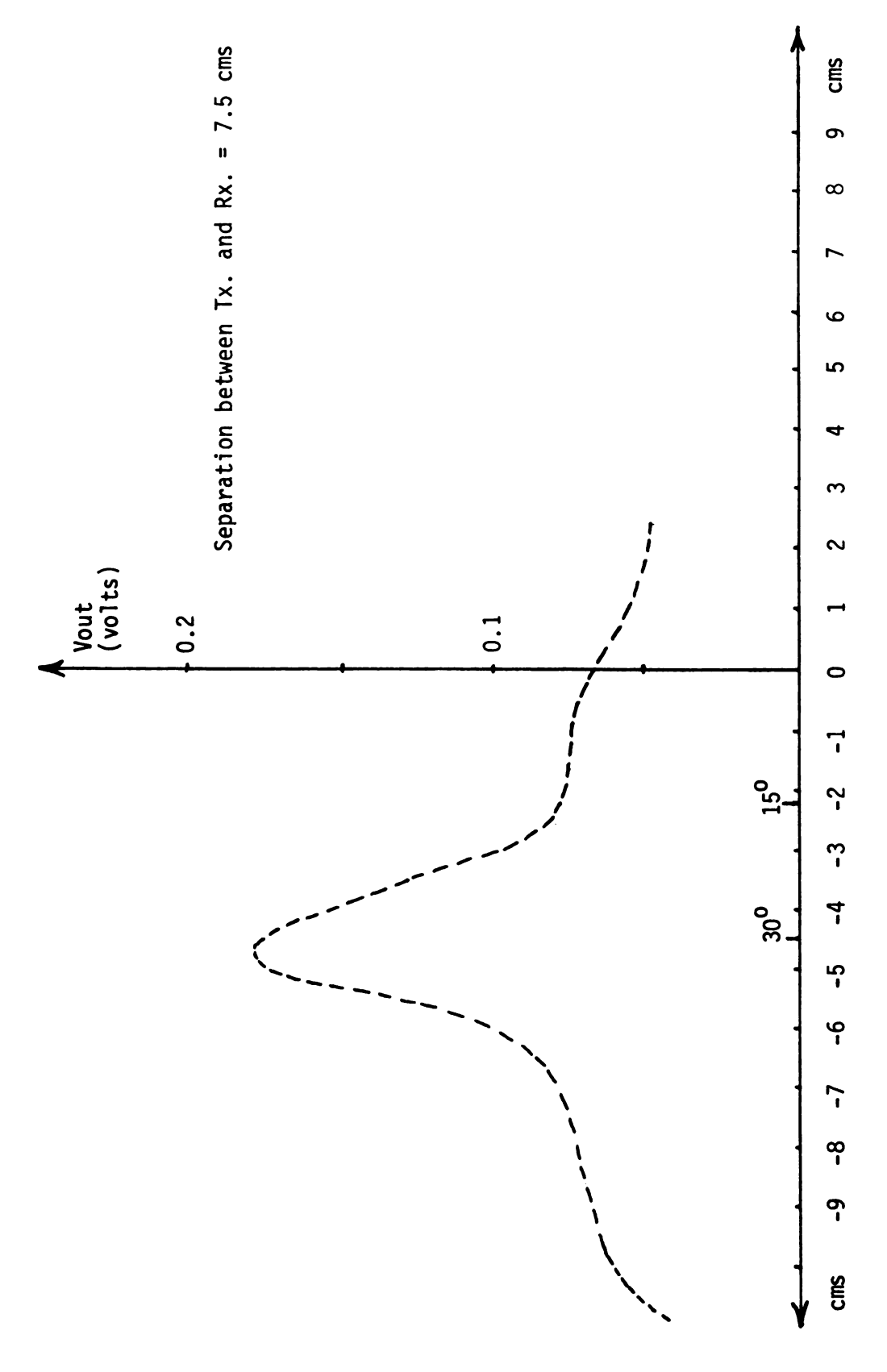


Figure 16 Plot of Vout vs Axial Displacement for Left Side Beam Steering

Amplitude of exciting pulses = 104 volts each

Noise level at the output = 0.03 volts

Table 9 Vout versus Axial Displacement for Left Side Beam Steering

	Axial Displacement (cms)	Peak to Peak Voltage Output Vout (volts)
1)	2.5	0.048
2)	1.5	0.052
3)	0.5	0.060
4)	0	0.065 (center of Tx.)
5)	-0.5	0.075
6)	-1.5	0.075
7)	-2.5	0.082
8)	-3.5	0.130
9)	-4.5	0.180 (peak of central lobe)
10)	-5.5	0.120
11)	-6.5	0.085
12)	-7.5	0.074
13)	-8.5	0.070
14)	-9.5	0.065
15)	-10.5	0.05

From this data the steering angle of the main lobe of ultrasound being transmitted can be calculated.

The shift in the position of central lobe, by applying a delay of 0.3 microseconds between each exciting pulse observed, = 4.5 cms

Separation between transmitter and receiver = 7.5 cms

So, $tan(\theta) = \frac{4.5}{7.5}$, θ being the observed steering angle $\theta = tan^{-1} \left(\frac{4.5}{7.5}\right) = 30.92$ degrees

Steering angle expected theoretically = 30 degrees

Experimental error = 0.92 degrees

This experiment is very similar to Experiment 3. The only difference between the two being that we want to steer the ultrasound beam by 30 degrees toward right rather than left along the axial axis 'x'. This can be achieved simply by operating the shift left/shift right switch on the programmable delay line to the shift right position. The data obtained is as follows: (See Figure 17 for plot.)

Separation between transmitter and receiver = 7.5 cms

Amplitude of exciting pulses = 104 volts each

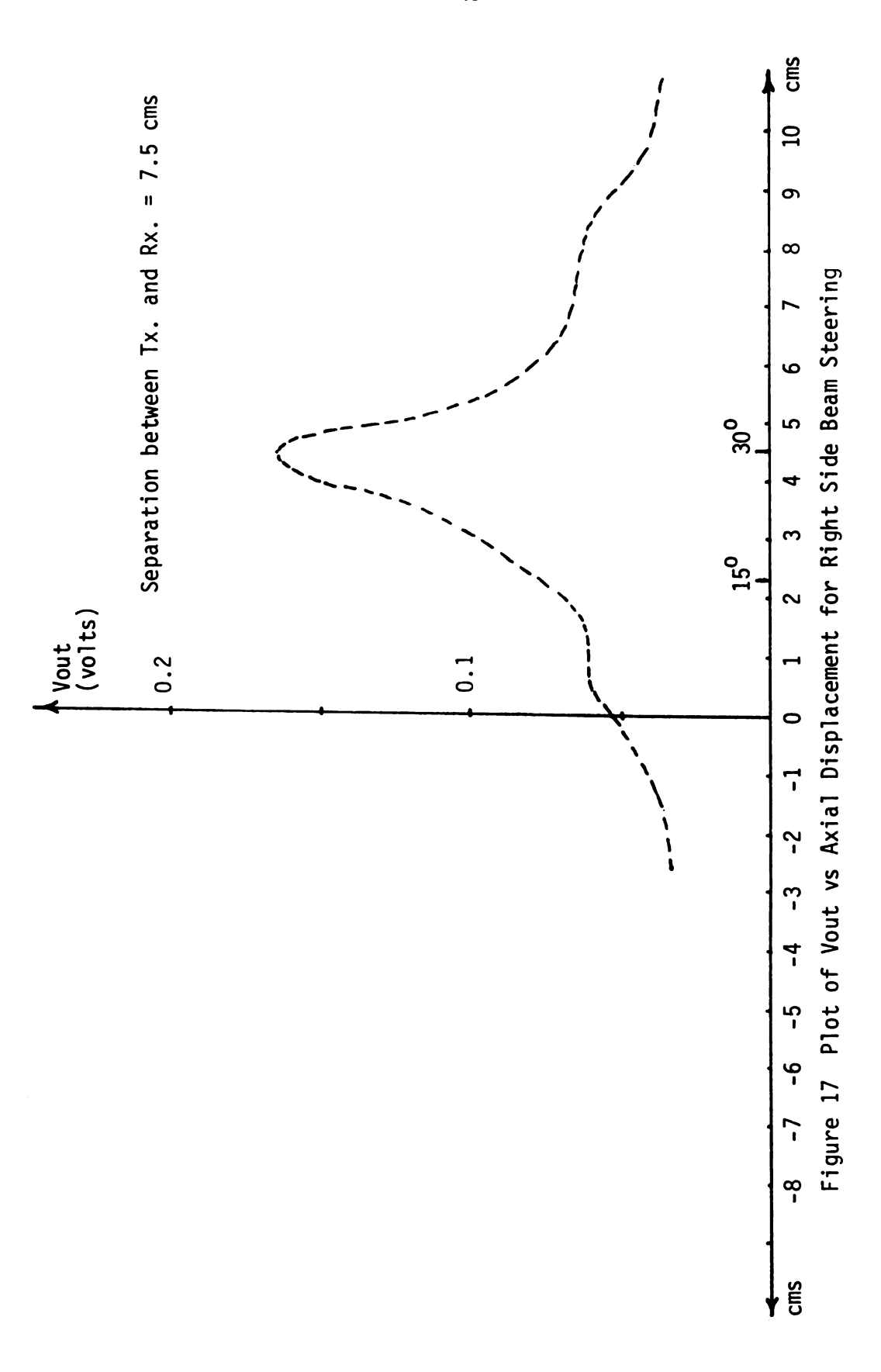
Noise level at the output = 0.03 volts

Table 10 Vout versus Axial Displacement for Right Side Beam Steering

-	Axial Displacement (cms)	Peak to Peak Voltage Output (volts)
1)	10.5	0.038
2)	9.5	0.045
3)	8.5	0.058
4)	7.5	0.062
5)	6.5	0.070
6)	5.5	0.095
7)	4.5	0.165 (peak of central lobe)
8)	3.5	0.100
9)	2.5	0.082
10)	1.5	0.06
11)	0.5	0.06
12)	0	0.052 (center of Tx.)
13)	-0.5	0.045
14)	-1.5	0.035
15)	-2.5	0.032

The steering angle can be calculated from this data very easily.

The shift in the position of central lobe by applying a delay of



0.3 microseconds between each exciting pulse observed = 4.5 cms

Separation between transmitter and receiver = 7.5 cms so, $\tan(\theta) = \frac{4.5}{7.5}$, θ being the observed steering angle $\theta = \tan^{-1}\left(\frac{4.5}{7.5}\right) = 30.92$ degrees

Steering angle expected theoretically = 30 degrees

Experimental error = 0.92 degrees

Experiment 5

This experiment is very similar to Experiment 3. We want to steer the ultrasound beam by 30 degrees towards left along the axial axis 'x'. The only difference being that the distance between transducer array transmitting ultrasound and the receiver has been increased to 10 centimeters so that we can have a better idea of how the field pattern varies as this distance is increased. The data obtained is as follows: (See Figure 18 for plot.)

Separation between transmitter and receiver = 10.00 cms

Amplitude of exciting pulses = 104 volts each

Noise level at the output = 0.03 volts

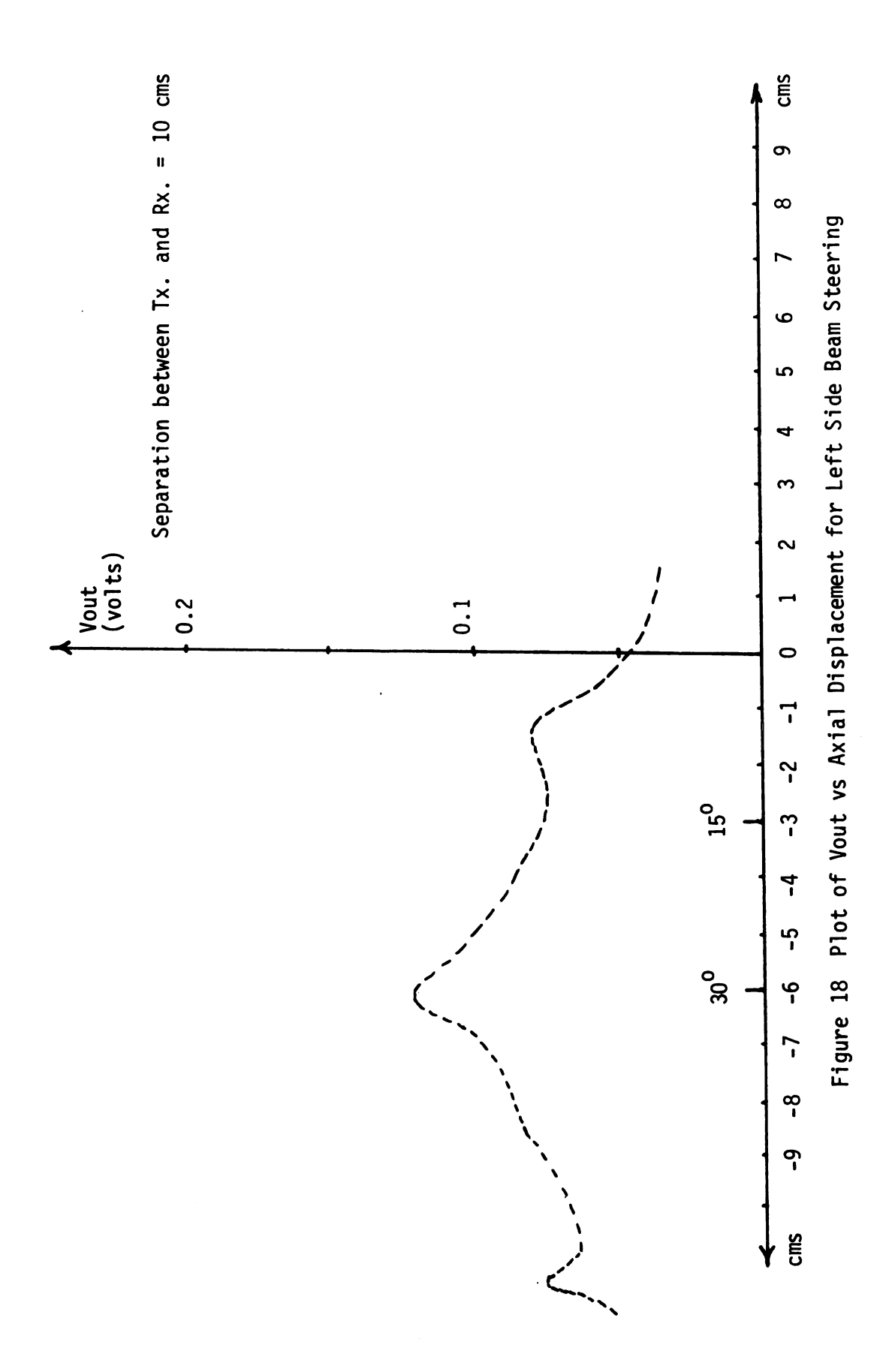


Table 11 Vout versus Axial Displacement for Left Side Beam Steering

	Axial Displacement (cms)	Peak to Peak Voltage Output (volts)
1)	1.5	0.035
2)	0.5	0.040
3)	0	0.050 (center of Tx.)
4)	-0.5	0.058
5)	-1.5	0.085
6)	-2.5	0.075
7)	-3.5	0.082
8)	-4.5	0.095
9)	-5.5	0.110
10)	-6.0	0.120 (peak of central lobe)
11)	-6.5	0.105
12)	-7.5	0.090
13)	-8.5	0.082
14)	-9.5	0.071
15)	-10.5	0.062
16)	-11.5	0.070
17)	-12.5	0.040

The steering angle can be calculated from this data as follows:

The shift in the position of central lobe by applying a delay of

0.3 microseconds between each exciting pulse observed = 6.0 cms

Separation between transmitter and receiver = 10.00 cms so

$$tan(\theta) = \frac{6.00}{10.00}$$
; θ being the observed steering angle

$$\theta = \tan^{-1}\left(\frac{6.00}{10.00}\right)$$

= 30.92 degrees

Steering angle expected theoretically = 30.00 degrees

Experimental error = 0.92 degrees

This experiment is very similar to Experiment 5. We want to steer the ultrasound beam by 30 degrees towards left along the axial axis 'x'. The only difference being that the distance between transducer array transmitting ultrasound and the receiver has been reduced to 5 centimeters so that we can have some idea of how field pattern of the steered ultrasound beam looks like near the transducer array. The data obtained is as follows: (See Figure 19 for plot.)

Separation between transmitter and receiver = 50 cms

Amplitude of exciting pulses = 104 volts each

Noise level at the output = 0.03 volts

Table 12 Vout versus Axial Displacement for Left Side Beam Steering

Axial Displacement (cms)	Peak to Peak Voltage Output (volts)
1.5	0.050
0.5	0.062
0	0.068 (center of Tx.)
-0.5	0.075
-1.0	0.080
-2.0	0.120
-2.5	0.180
-3.0	0.220 (peak of central lobe)
-3.5	0.170
-4.0	0.105
-5.0	0.080
-6.0	0.072
-7. 0	0.065
-8.0	0.060
-9.0	0.055
-10.0	0.046
-11.0	0.042
	(cms) 1.5 0.5 0 -0.5 -1.0 -2.0 -2.5 -3.0 -3.5 -4.0 -5.0 -6.0 -7.0 -8.0 -9.0 -10.0

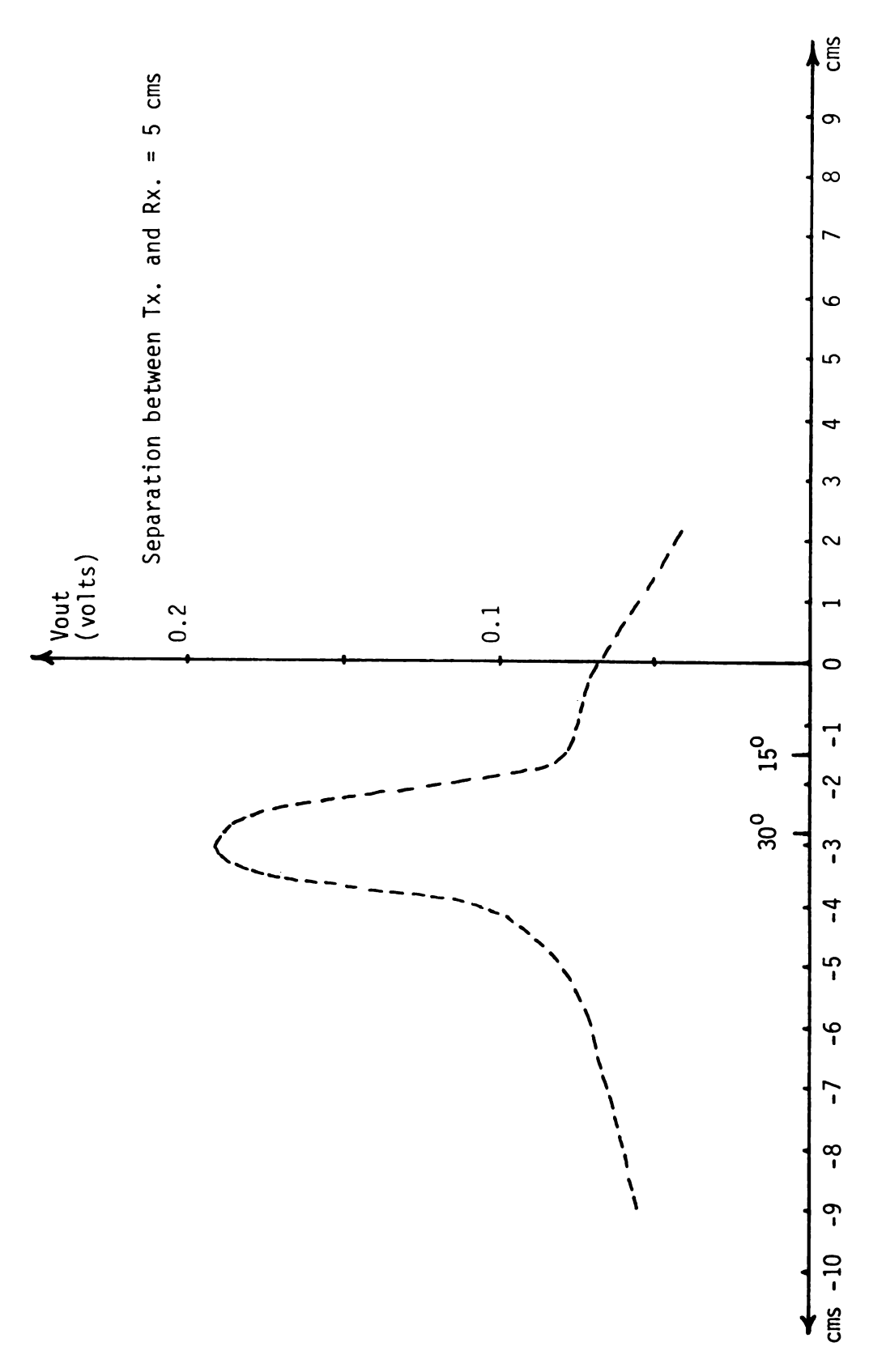


Figure 19 Plot of Vout vs Axial Displacement for Left Side Beam Steering

The steering angle can be calculated from this data as follows:

The shift in the position of the central lobe by applying a delay of 0.3 microsecond between each exciting pulse observed = 3.0 cms

Separation between transmitter and receiver = 5.0 cms so,

 $tan(\theta) = \frac{3.00}{5.00}$; θ being the observed steering angle.

$$\theta = \tan^{-1}\left(\frac{3.00}{5.00}\right)$$

= 30.92 degrees

Steering angle expected theoretically = 30.00 degrees

Experimental error = 0.92 degrees

CHAPTER V CROSS COUPLING

Piezoelectric transducer arrays normally consist of closely packed radiating elements separated by a distance smaller than half the wavelength of fundamental resonance frequency. This is a fundamental requirement in the ultrasonic array design, but on the other hand, it brings along with it the cross coupling problem.

Cross coupling is a phenomona which describes the influence of an excited element on the neighboring elements due to induction. Cross coupling may, in fact, have an appreciable effect on the field strength pattern. In the near field this effect can be easily observed, but in the far field it can also be seen. It will also arise from the fact that the individual array elements reside on a common piezoelectric base. These may be minimized by shielding the wires and minimizing base thickness. However, even if these sources of cross coupling were completely eliminated, appreciable cross coupling would still exist as is seen in the analysis below which closely follows the analysis of Wei Ming Wang. (1) This Chapter describes some theoretical aspects of cross coupling.

The theoretical analysis in this Chapter is based on the assumption that only one element is excited at a time and its effect, with regard to coupling, is observed on the neighboring elements. Under this assumption, cross coupling will have two componants, one is due to the direct reception of the spherical waves at the receiving element being generated

by the excited element and the second is due to reflected wave componant from the boundary of any object obstructing the propagation of ultrasonic waves. The boundary conditions of the reflecting medium become excessively important for this componant for the case where the medium is not well defined (like a body). In order to deal with such situations, an assumption is made that considers the reflected wave componant being generated by a ficticious 'image source' formed at the same distance as the actual source is from the reflecting boundary, as shown in the Figure 23. All elements are considered to be similar and resonate at the same frequency.

Consider the induced voltage at an element due to a neighboring excited element. The electro-mechanical equivalent circuit of each element is shown in the Figure 20 (2) where

Z_o is output impedance

 $\mathbf{Z}_{\mathbf{m}}$ is the short circuit mechanical impedance

 $Z_{\mathbf{p}}$ is the input electrical impedance

 $\mathbf{Z}_{\mathbf{S}}$ is the impedance of the voltage source

 Φ is the transformation ratio. This ratio basically describes the conversion ratio of electrical excitation to mechanical stress wave generated by the transducer.

From the equivalent circuit of Figure 20 we note that $\mathbf{Z}_{\mathbf{0}}$ impedance is given as

$$Z_0 = (Z_s Z_e/Z_e + Z_s) \Phi^2 + Z_m$$
 and $V_1 = (Z_e/Z_e + Z_s) E_s$ so V_{00} (open circuit) = ΦV_1

For the above circuit a Norton's equivalent circuit can also be drawn as shown in the Figure 21, where

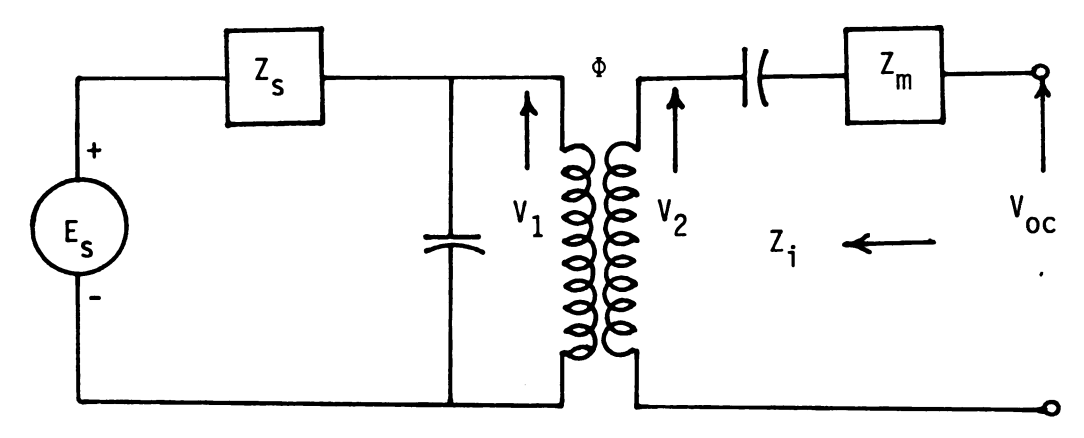


Figure 20 Equivalent Circuit Model of an Array Element

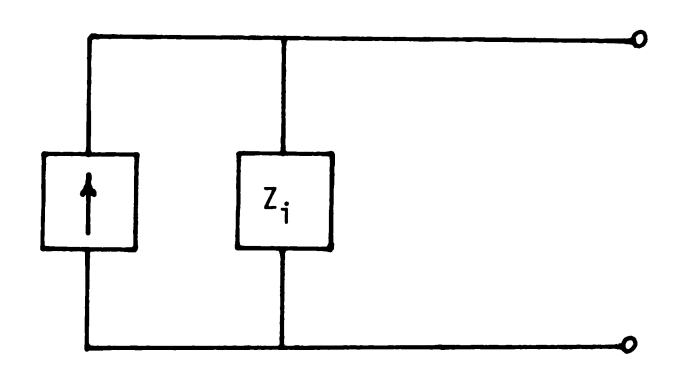


Figure 21 Norton's Equivalent Model of an Array Element

$$I(norton) = (Z_e/Z_s + Z_e)E_s \Phi / \frac{(Z_sZ_e)}{Z_s+Z_e} \Phi^2 + Z_m$$
$$= Z_e E_s \Phi / (Z_s + Z_e)Z_0$$

I(norton) is a current source in the circuit, but from the transmission line analogy it is in fact a velocity source because the transducer element is generating an ultrasonic stress wave traveling at a certain velocity in the medium. So, I(norton) can be replaced by ${}^{\mathsf{V}}_{\mathsf{O}}{}^{\mathsf{I}}$ in the above expression; where ${}^{\mathsf{V}}_{\mathsf{O}}{}^{\mathsf{I}}$ represents the velocity of ultrasonic stress wave, so

$$V_0 = Z_e Z_s \Phi / (Z_e + Z_s) Z_o$$

Let 'V' be the induced velocity in the nth element due to the radiating element. This induced velocity is due to the induced wave in the secondary side of the receiver equivalent circuit as shown in the Figure 22. So, the induced voltage can be found out in the primary circuit.

E ind. =
$$I_1 (Z_e Z_s / Z_s + Z_e)$$

where \mathbf{I}_1 is the current in the primary circuit due to induced current \mathbf{I}_2 so

E ind. =
$$(\Phi I_2)(Z_2Z_5/Z_5 + Z_6)$$

or in terms of the acoustic analogy, we can replace induced current I_2 by the induced velocity 'v'. So,

E ind. =
$$(\Phi v)(Z_eZ_s/Z_e + Z_s)$$

The expression for the induced velocity can now be derived under certain assumptions. The most important of all being that although the generated and received waves are spherical or semi-spherical in nature we can treat them as plane waves for the reason that the reflecting plane is at a number of wavelengths away from the source (far field approximation).

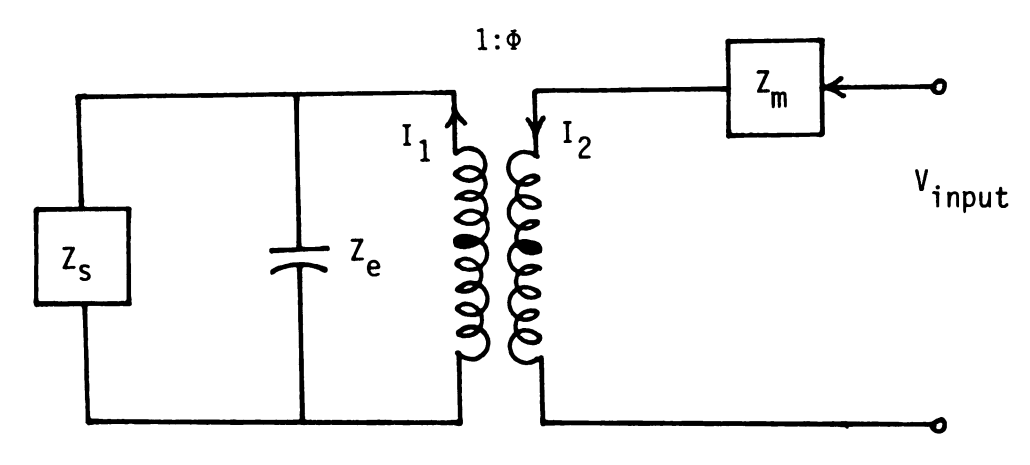


Figure 22 Receiving Element Equivalent Circuit

So, under this assumption the stress exerted by the transmitted wave on the receiving element is given as

F = P * A * D where

P = Acoustic pressure at the center of the receiving element

A = Face area of the element

D = Directivity function of the element face

As the dimension of the elements are smaller than the wave length we can approximate the expressions of 'P' and 'D' by the standard expression of P and D for a circular transducer. Using these standard expressions, a standard expression for induced stress can be found and using the concept that the total stress wave reaching the receiver element is the sum of direct plane wave plus the reflected plane wave from the reflecting medium, the second part of received wave can be approximated by a plane wave generated by a fictitious source, as shown in Figure 23, to meet the non-uniform reflecting conditions of the obstructing medium; one can derive the expression for the induced velocity, (3) the result stated below for the induced velocity for a receiving element when only one element in the whole array is excited.

$$V = VoA^2D^2(-iw\rho e^{ikr}F(\rho))/2\pi r_1Z_0$$
 where

 $\label{eq:Vo_state} \mbox{Vo = Velocity of ultrasound waves in the medium under consideration}$

A = Face area of the element

D = Directivity function of the receiver element face

w = Frequency of the ultrasound waves

 ρ = Numerical distance

=
$$ikr_2(\gamma 0 + \beta 0)^2/(1 + \gamma 0 \beta 0)^2$$
 where

 ${\bf k}$ and ${\bf r}_2$ represent distances shown in the Figure 23

 $\gamma o = \cos (Angle \ of \ incidence)$

 $\gamma o = \cos(\theta o)$

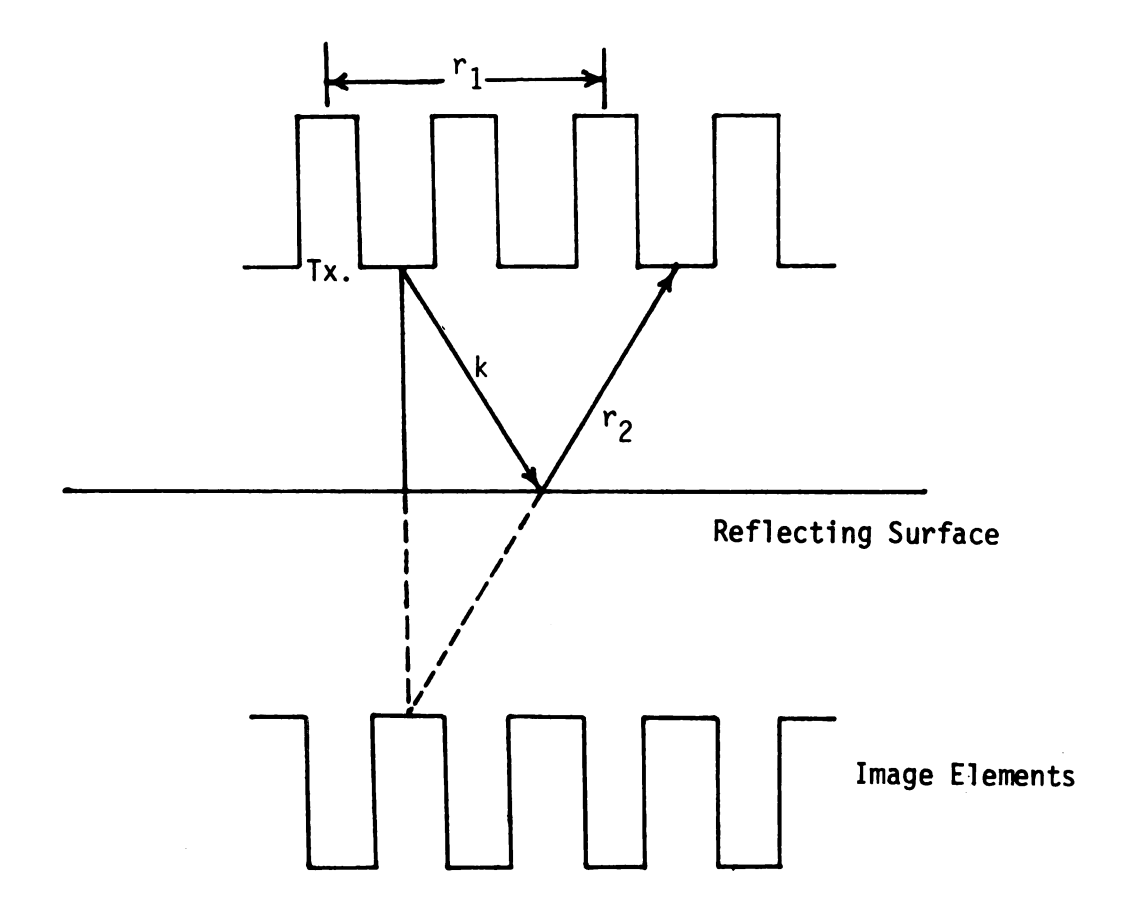


Figure 23 Plane Wave Model of a Transmitting/Receiving Element of an Array

Bo = acoustic admittance

 $F(\rho)$ = error function introduced to compensate for plane wave assumption

If more than one element is radiating then this induced voltage will be the summation of induced voltage componants due to each element.

This is a generalized expression for a case where the elements are separated from each other. For the case where the elements are joined by a common substrate of piezoelectric material, another componant due to mutual induction between the elements should be added to find out the induced velocity.

The conclusion, which can be drawn from this mathematical analysis, is that the induced voltage is inversely proportional to the center to center distance between the transmitting and the receiving elements. The effect of this cross coupling is considerable in the near field in comparison to the far field. As most of the observations are normally taken in the far field, these cross coupling effects are given a secondary importance in the design. If, in fact, appreciable cross coupling is observed in the far field, it may be due to a "non-ideal" form of cross coupling, such as the common base or intra-wire coupling.

5.1 Experimental Results

In order to study the effect of cross coupling on the transducer array fabricated during this research, three similar experiments were

performed. In all these experiments one of the elements of the array is excited by a voltage pulse of the same amplitude as was used in all six experiments of Group 2 in Chapter 4, and the induced voltage is measured at the terminals of other elements.

Experiment 1

In this experiment the central element '4' (see Figure 9, Chapter 3 for element numbering) of the array was excited by a 0.3 microsecond pulse and the induced voltages on other elements of the array were observed. The data obtained is listed below:

Amplitude of the exciting pulse = 104 volts

Element excited = No. 4

Table 13 Induced Voltage for Different Elements of the Array

Element Number	Induced Voltage (volts)	
1	5.20	
2	7.0	
3	8.0	
5	7.90	
6	6.75	
7	5.00	

Experiment 2

In this experiment, the first element '1' (see Figure 9, Chapter 3 for element numbering) of the array was excited by a 0.3 microsecond pulse and the induced voltages on other elements of the array were observed. The data obtained is listed below:

Amplitude of the exciting pulse = 104 volts

Element excited = No. 1

Table 14 Induced Voltage for Different Elements of the Array

Element Number	Induced Voltage (volts)	
2	10.00	
3	7.20	
4	5.10	
5	3.50	
6	3.00	
7	2.80	

Experiment 3

In this experiment, the last element '7' (see Figure 9, Chapter 3 for element numbering) of the array was excited by a 0.3 microsecond pulse and the induced voltages on other elements of the array were observed. The data obtained is listed below:

Amplitude of the exciting pulse = 104 volts

Element excited = No. 7

Table 15 Induced Voltage for Different Elements of the Array

Element Number	Induced Voltage (volts)	
1	2.9	
2	3.05	
3	3.50	
4	4.95	
5	6.85	
6	9.50	

CHAPTER VI CONCLUSIONS

The experimental results obtained in general for the field strength pattern of the array and the steering data obtained agrees well in some aspects with the theoretical predictions of Chapter 2. However, there are important differences too. Following are some conclusions which can be drawn by comparison of theoretical results and experimental data:

- 1) The experimental field strength pattern of the array with all elements excited at the same time, shown in Figure 14, seems to be agreeing in general with the theoretical field strength pattern of Figure 3; both have a main lobe and two major side lobes. However, a close study indicates marked differences in the ratio of main lobe height to side lobe height, the width of main lobes, the position of side lobes and a missing pair of first side lobes. The theoretical ratio of main lobe to side lobe height was 1.37 to the observed ratio of 3.07. The theoretical width of the main lobe was 25 degrees to the observed width of 58 degrees and the theoretical position of the first side lobe was 20 degrees to the observed first side lobe of 36 degrees.
- 2) The experimental field strength pattern of the central element of the array, shown in Figures 12 and 15, does not closely agree with the theoretical field strength pattern of Figure 4. The difference is that we expected the field strength pattern to be much flatter than what we observed experimentally.

- One reason for deviation between theory and experiment may be fabrication flaws, such as non-uniform solder connections between the elements of the array and the external connecting wires. Also we could probably get better results by reducing the common substrate coupling during fabrication.
- 3) The observed angle of beam steering agrees quite closely with that predicted theoretically as may be seen from a study of the beam steering Experiments 3, 4, 5, and 6 of Group 2 in Chapter 4. The experimental results show that by exciting the elements by sharp pulses of 0.3 microsecond duration, each being delayed by 0.3 microseconds from its proceeding pulse, we can steer the beam left or right along the axial axis through an angle of 30.92 degrees (see calculations for Experiments 3, 4, 5, and 6, Group 2, Chapter 4) whereas the theoretical steering angle expected is 30.00 degrees. The experimental error in the steering angle, which is the difference between experimental and theoretical steering angles, may be due to the fact that one of the central elements of the array went out of operation during testing or may be due to dissymmetries in the elements of the fabricated array. Again, the ratio of side lobe height to main lobe height is higher than the theoretically predicted value.
- 4) The programmable delay line developed during the course of this research is capable of steering the ultrasound beam through discrete angles between 0 degrees and ± 45 degrees. Using the programmable delay line in automode (DECX control), gates and power amplifiers, the ultrasound beam should be steerable through angles between 0 and ± 45 degrees in steps of 2 degrees under the

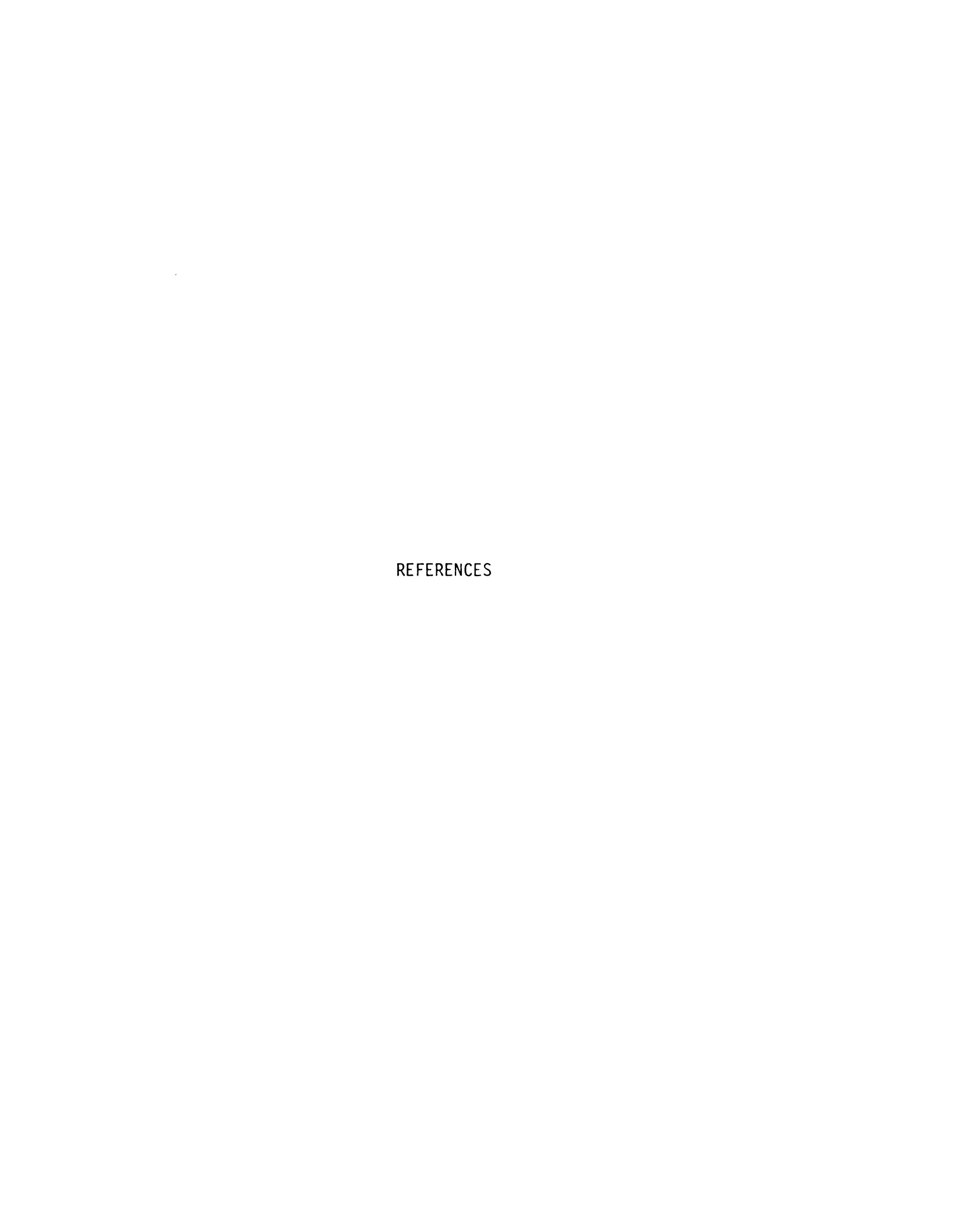
- computer control. However, computer control was not actually exercised because a key high speed IC chip was not yet in hand at the time of taking data. Finer angular resolution is obtainable by extension of the design to higher clock frequencies.
- 5) The peak to peak output voltage obtained during Experiments 3, 5, and 6 of Group 2 leads to the conclusion that the field strength varies as R^{-2} , where R is the distance between transmitter and the receiver. However, the main lobe to side lobe height ratio does not remain constant as expected theoretically; it also decreases with field strength as the distance between transmitter and receiver is increased. This may be due to the fact that the field strength pattern of each element is not as flat as expected. At present, this remains an unanswered question. Also, a R^{-1} dependence was expected rather than a R^{-2} dependence observed.
- 6) The data obtained during Experiments 1, 2, and 3 of Chapter 5 (Cross Coupling) leads to the conclusion that the induced voltage varies somewhere between d⁻¹ to d^{-0.67}, where d is the axial distance between transmission and reception points; whereas, a d⁻¹ dependence was predicted in Chapter 5. However, an exact agreement should not be expected due to the presence of other components of cross coupling. Since the excitation pulse was quite short (0.3 microseconds) in duration, it seems like the reflection contribution was quite small and it was probably due to the reflection near the transducer face such as transducer-medium boundary. The other components contributing towards

cross coupling were probably the common substrate induction and the intra-wire coupling componants.

CHAPTER VII RECOMMENDATIONS

Keeping in view the conclusions, the following recommendations are proposed for future research.

- 1) The fabrication process proposed in Chapter 3 can be improved by applying deeper cuts for separating the elements. This would reduce the common substrate induction, subsequently reducing the cross coupling. A better technique should be developed for solder connections between the array elements and the external wires. The external wires must also be shielded throughout to reduce intra-wire coupling.
- 2) In order to improve dynamic range (ratio of main lobe height to side lobe height) and lateral resolution in the far field, arrays with a larger number of elements should be fabricated. Commercial units have on the order of 20 elements.
- 3) The reduction of main lobe height to side lobe height with the increase of distnce between transmitter and receiver is also one of the aspects to be studied in detail.
- 4) The central element of the transmitting array could also be used as a receiver. More ideally, if all elements receive with the same directionality as they transmit better dynamic range is achievable. This is done in current commercial units by Grumman and Varian, for example.



REFERENCES

CHAPTER I

- 1) Harry E. Thomas, "Handbook of Biomedical Instrumentation and Measurement," Prentice-Hall Company, 1975, pp. 2-5.
- 2) A. A. Oliner and G. H. Knittel, "Phased Array Antennas," Artec House, Inc., 1970, pp. 1-7.
- 3) G. L. Gooberman, "Ultrasonic Theory and Applications," English Universities Press LTD., 1968, pp. 52-55.
- 4) H. G. Wells, "Ultrasound Applications," Plenum Press, 1965, pp. 17-24.

CHAPTER II

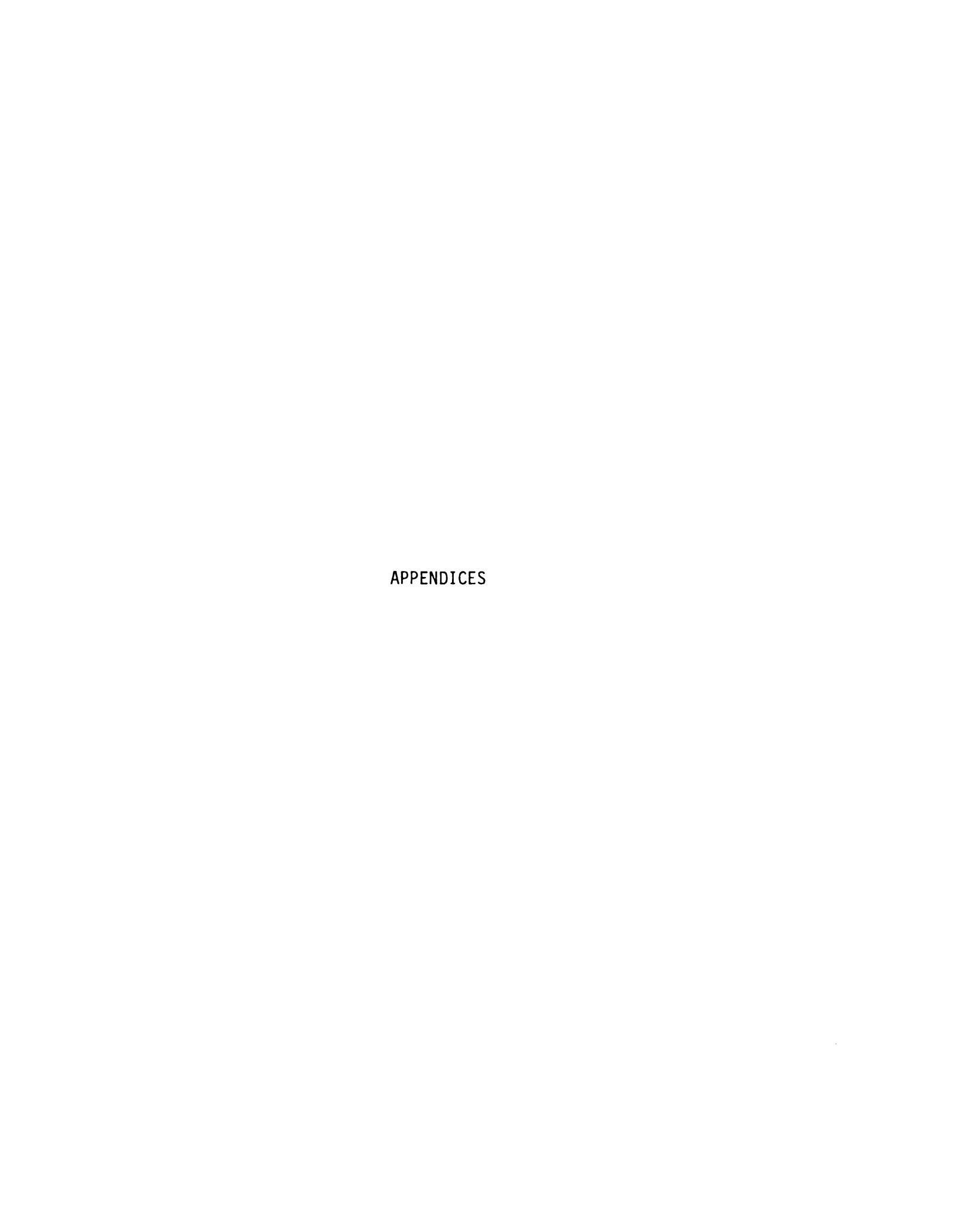
- 1) A. A. Oliner and G. H. Knittel, "Phased Array Antennas," Artec House, Inc., 1970, pp. 4-10
- 2) B. P. Hildebrand and B. B. Breden, "An Introduction to Acoustical Holography," Plenum Press, 1972, pp. 16-19.
- 3) O. L. Bobikov, "Ultrasonics and its Industrial Applications," Consultants Bureau NY, 1960, pp. 56-64.
- 4) G. L. Gooberman, "Ultrasonic Theory and Applications," English Universities Press LTD, 1968, pp. 54-59.
- 5) Glen Wade, "Acoustical Imaging," Plenum Press NY, 1975, pp. 111-126.
- 6) M. I. Skolnik, "Introduction to Radar Systems," McGraw-Hill Company, 1962, pp. 101-106.
- 7) "Ultrasonics in Medicine, Conference Papers," Munchen, 1975, pp. 75-80.
- 8) Yoshimitsu Kikuchi, "Ultrasonic Transducer," Corona Publishing Company, LTD, 1969, pp. 240-244.

CHAPTER V

- 1) Wei Ming Wang, "Mutual Coupling through Radiation Transducer Elements in an Infinite Array," IEEE Sonics, 1972, pp. 28-31
- 2) Charles Sherman, "Analysis of Acoustic Interactions in the Transducer Arrays," IEEE Sonics, 1966, pp. 9-15.
- 3) Uno Ingard, "On the Reflection of a Spherical Sound Wave from an Infinite Plane Wave," Journal of the Acoustical Society, 1951, pp. 329-335.

APPENDIX B

James F. Gibbons, "Physics of Semiconductor Devices," McGraw-Hill Company, 1965, pp. 275-325.



APPENDIX A PROGRAMMABLE DELAY LINE

APPENDIX A

Programmable Delay Line

The programmable delay line can be used to produce a number of delay outputs upon initiation by an excitaion pulse. The time delay between the output can be controlled in a predetermined fashion. A programmable delay line was designed and developed during the course of this research. The initial design was originated by Mr. Philip Chimento, and was completed by the author with consultation by Mr. Mark Funk. The details of that are given below and shown in Figure 24.

There are two modes of operation of this programmable delay line, namely the manual and auto mode. In manual mode of operation, the delay provided between the output pulses is controlled by six single pull double throw switches and in auto mode the computer controls the delays through its control signal called DECX. The delay line is initiated by the inverted DECX signal which allows the AND gate 1 to open and allows the upper counter to count the clock pulses. The frequency of the clock determines the minimum time delay between two consecutive outputs of the delay line. The outputs of the upper counter are applied to an equality gate (combination of XOR's and AND gate) along with the other outputs coming from the presettable counter, shown in the bottom part of the Figure. The outputs of this counter can be set to a predetermined value by setting the six single pull double throw switches in manual mode and operating the count/load momentary switch, or it can

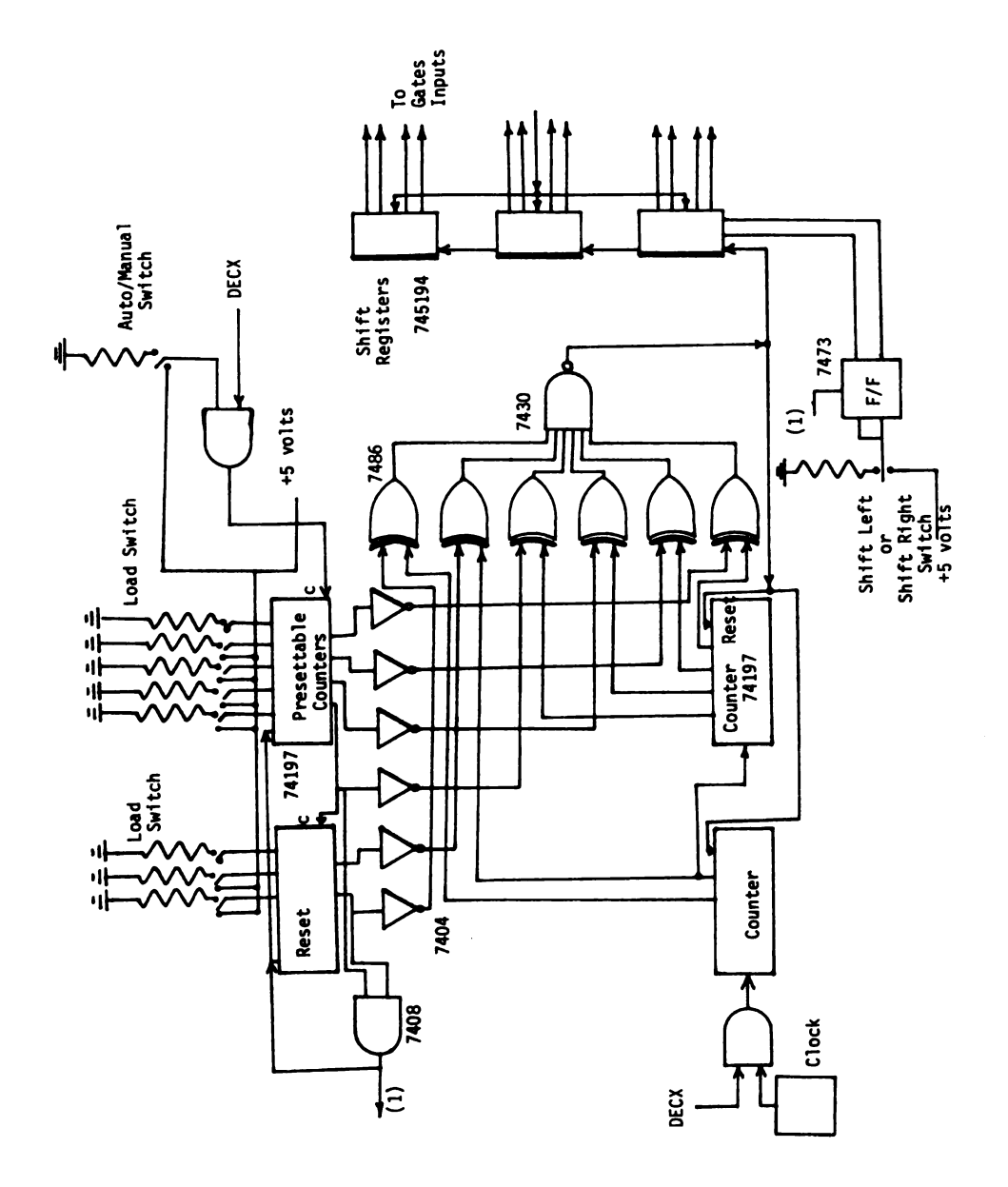


Figure 24 Programmable Delay Line

be set to count the DECX pulses in the auto mode. In the equality gate these two outputs of the top counter, counting clock pulses, and the presettable counter are compared and it will give an output pulse whenever the two counts become equal. This output is applied as a clock pulse to shift registers. In this way the output of the equality gate is used to shift one's throw shift registers. Before this pulse appears the shift register outputs are zero's. When the first pulse appears the first output bit of shift registers go high, on second pulse from equality gate the second output bit goes high and so on. It is obvious from this description that the time interval between two consecutive output bits depends upon the time interval between two consecutive equality gate output pulses.

The shift registers are dual type and can shift the data right or left. The mode of operation of shift registers (left or right shift) depends upon its inputs S_0 and S_1 . Shifting the data left means we want to steer the beam towards left side from the control position of the beam. The inputs S_0 and S_1 are controlled by the outputs from a flip flop, whose operation is controlled by an external single pull double throw switch. When this external switch is in position '1' the outputs S_0 and S_1 are at levels '0' and '1' respectively and so the data in the shift registers starts moving left. When this switch is in position '2' the outputs of the flip flop S_0 and S_1 are at levels '1' and '0' respectively and in this case the data will be moved towards the right. Therefore, by controlling the position of this switch the outputs of the shift registers can be obtained either from least significant bit to least significant bit (shift left) or from most significant bit to least significant bit (shift right). Each output bit of

shift registers controls the initiation of excitation of one element of the transducer array. Once the data is shifted from right to left or from left to right completely, meaning that all output bits have '1's at their terminals, no more data can be shifted before clearing the shift registers. The same DECX pulse which starts the operation of this delay line is used to clear the shift registers so that by the time the equality gate starts giving output the shift registers are ready to accept new data from it. The programmable delay line developed has a maximum capability of 10 output bits, which means that an ultrasonic transducer array with 10 elements can be excited by this delay line.

The limitations of this circuit is that in auto mode it can steer the beam only by $^{\pm}40$ degrees from the central position of the main lobe. In order to do so the 4th and 6th bits of the presettable counter is connected to the AND gate '2' as shown in the Figure. The output of this AND gate resets the presettable counters and also changes the state of the flip flop controlling the shift left shift right operation of the shift registers. In this way, after steering the beam in one direction by 40 degrees, this delay line starts steering the beam in the other direction till it reaches 40 degrees beam shift and then the whole cycle is repeated again.

APPENDIX B GATES AND POWER AMPLIFIERS

APPENDIX B

Gates and Power Amplifiers

The outputs of the programmable delay line are levels rather than pulses in the manual mode and are pulses of low frequency in case of the auto mode, so one needs some kind of short pulse generating circuit to operate at the beginning of each level shift ('0' to '1') of the output bits of shift registers. A monostable circuit can be used for generating sharp pulses at the beginning of each level shift. However, the monostable circuit has a low fan out and is not capable of supplying enough current to the power amplifiers without considerably loading itself. Digital multiplexing gates can be used to solve this problem of loading with their continuous input being connected to +5 volts and the control input to the monostable output. The output of the gates can not be connected to the inputs of the power amplifiers.

The power amplifiers are needed to amplify the low voltage pulse generated by the monostables. This is necessary because one needs a high power pulse to excite the transducer elements. For this purpose a cascaded power amplifier with two stages was designed. (See Figure 26.) The coupling capacitor and 470 Ω 's resistance forms a filtering network which eliminates the small leakage spikes coming from the presettable counter. The first stage is a common emitter configuration to give the necessary voltage gain to the input signal. The second stage is a direct coupled common collector stage to provide the necessary

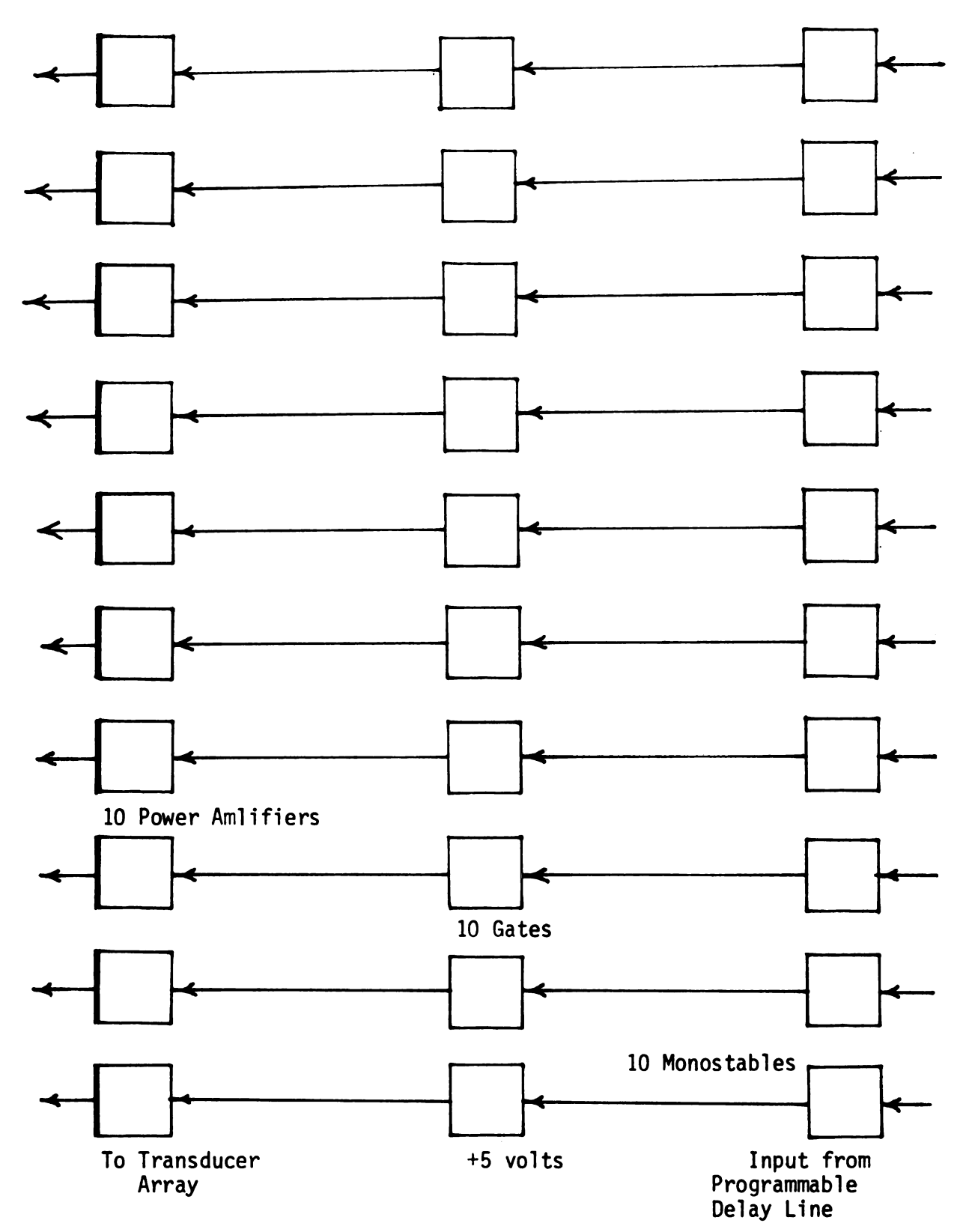


Figure 25 Block Diagram of Gates and Power Amplifier

high current gain so that the amplifier can supply large currents to the load (array elements) without loading the common emitter stage. During the course of this research, seven such cascaded amplifiers (one for each element) were designed using the standard formulae (1) and the circuit diagram of one of such amplifiers is shown in Figure 26.

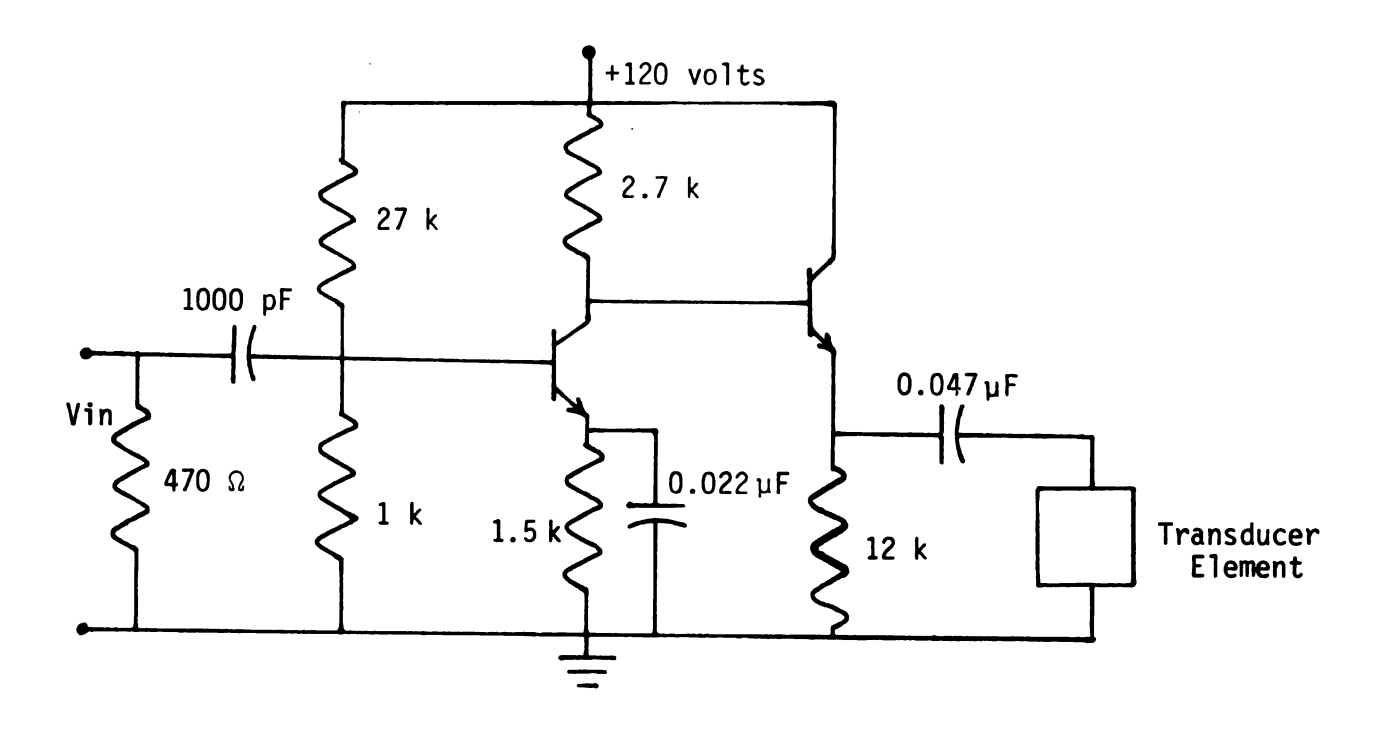


Figure 26 Circuit Diagram of Power Amplifier

APPENDIX C
COMPUTER PROGRAMS

APPENDIX C

Computer Programs

This appendix includes the computer programs developed for simulating the steering and focusing effects of the ultrasonic transducer array.

The Program 1 listed below is for steering and Program 2 is for focusing effect simulation.

Program 1 (VORTXII FTN IV(G) SAEED)

```
2 C DESIGN OF PHASED ARRAY FOR RECONSTRUCTIVE TOMOGRAPHY
```

- 3 C DATA VARIABLES ARE AS FOLLOWS
- 4 C D = SPACING OF ELEMENTS
- 5 C V = VELOCITY OF ULTRASONICS IN THE MEDIUM UNDER CONSIDERATION
- 6 C F = FREQUENCY OF ULTRASONICS
- 7 C N = NUMBER OF ARRAY ELEMENTS
- 8 C A = WIDTH OF ONE ARRAY ELEMENT
- 9 C T = TIME DELAY OF EXCITATION
- 10 C THETA = ANGLE OF MAIN LOBE WITH NORMAL
- 11 REAL LAMBDA
- 12 DIMENSION P(150), IP(2), D(2), ID(2)
- DATA (ID(I), I = 1, 2)/1 HP, 2 HPD/
- 14 READ (4, 10) B, V, F, N, A, T
- 15 WRITE (5, 10) B, V, F, N, A, T
- 16 10 FORMAT (F10.0, 2E10.3, I5, 5X, 2F10.0)
- 18 IP (2) = 1
- 19 D(1) = 1
- 20 D(2) = 1
- 21 THETA = -60
- 22 PHI = 3.14592

```
23
           LAMBDA = (V/F)
24
           NI = N
25
           DO 20 I = 1,121
26
           TETA = (THETA * PHI/180.)
           X = SIN (TETA)
27
28
           THERD = (PHI * SIN (TETA)/LAMBDA)
29
           U = (THERD * B)
30
           UP = (THERD * A)
31
           UF = (PHI * T * F)
32
           UT = (U - UF)
33
           US = FLOAT (NI) * UT
34
           UR = (SIN (US))
35
           P1 = SIN (UP)/UP
           P2 = SIN (US)/SIN(UT)
36
37
           IF (P1. GT. 1) GO TO 100
38
           IF (P2. GT. NI) GO TO 200
39
           GO TO 80
40
    100
           P1 = 1
41
           IF (P2. GT. NI) GO TO 150
42
           P2 = SIN (US)/SIN (UT)
43
           P(I) = P1 * P2
44
           GO TO 85
    200
           P2 = NI
45
46
           P1 = SIN (UP)/UP
           P(I) = P1 * P2
47
48
           GO TO 85
49
    150
           P1 = 1
50
           P2 = NI
51
           P(I) = P1 * P2
52
           GO TO 85
53
           P(I) = P1 * P2
     80
54
     85
           PDB = (20.0 * ALOG 10 (ABS (P(I)/NI)))
55
           WRITE (5, 50) THETA, P(I), PDB, P1, P2
56
     50
           FORMAT (5(F10.6, 5X))
57
     60
           THETA = THETA + 1.0
58
           WRITE (8) THETA, P (I), PDB
59
     20
           CONTINUE
```

```
Program 2 VORTXII FIN IV(G) SAEED
```

```
FOCUSING EFFECT SIMULATION FOR SECOND PHASED ARRAY
2 C
3 C
             Z = FOCAL POINT
4 C
              D = ELEMENT TO ELEMENT DISTANCE
5 C
             Y = DEPTH OF MEASUREMENT
6
         REAL LAMBDA
7
         DIMENSION P(100), IP(2), DD(2), ID(2), L(4), M(4), I(4), PHE(4)
8
         DATA (ID(I), I = 1, 2)/1HP, 2HPD/
9
         READ (4, 10) D, Z, V, F, Y
         WRITE (5, 10) D, Z, V, F, Y
10
         FORMAT (2F10.0, 2E10.3, F10.0)
11
   10
12
         IP(1) = 1
         IP(2) = 1
13
         DD(1) = 1
14
15
         DD(2) = 1
16
         A = 0.4
17
         N = 7
18
         X = -100
19
         PHI = 3.141592
20
         LAMBDA = (V/F)
21
         L(1) = (3.0 * D)
22
         L(2) = (2.0 * D)
23
         L(3) = D
24
         D0 20 I = 1, 3
25
         M(I) = L(I) * SIN(ATAN(L(I)/Z))
         T(I) = M(I)/V
26
27
         PHE (I) = (T (I) * 2 * PHI 8 F)
28
         CONTINUE
   20
29
         DO 30 J = 1, 41
         R = ((X * * 2.0 + Y * * 2.0) * * 0.5)
30
         R1 = ((((X + 3.0 * D) * * 2.0) + Y * * 2.0) * * 0.5)
31
32
         R2 = ((((X + 2.0 * D) * * 2.0) + Y * * 2.0) * * 0.5)
33
         R3 = ((((X + D) * * 2.0) + Y * * 2.0) * * 0.5)
34
         R4 = ((((X - D) * * 2.0) + Y * * 2.0) * * 0.5)
         R5 = ((((X - 2.0 * D) * * 2.0) + Y * * 2.0) * * 0.5)
35
         R6 = ((((X - 3.0 * D) * * 2.0) + Y * * 2.0) * * 0.5)
36
```

```
37
         E1 = ((2.0 * PHI * (R1 - R))/LAMBDA
         E2 = PHE (1) + ((2.0 * PHI * (R2 - R))/LAMBDA
38
         E3 = PHE (2) + ((2.0 * PHI * (R3 - R))/LAMBDA
39
         E4 = PHE (3)
40
         E5 = PHE (2) + ((2.0 * PHI * (R4 - R))/LAMBDA
41
42
         E6 = PHE (1) + ((2.0 * PHI * (R5 - R))/LAMBDA
43
         E7 = ((2.0 * PHI * (R6 - R))/LAMBDA
         P1 = (COS (E1/R1) + COS (E2/R2) + COS (E3/R3) + COS (E4/R))
44
45
         P2 = (COS (E5/R4) + COS (E6/R5) + COS (E7/R6))
46
         P4 = P1 + P2
         IF (X. EQ. 0) TH = PHI/2.0
47
         IF (X. NE. O) TH = ATAN (Y/X)
48
         THERD = PHI * SIN (TH)/LAMBDA
49
         UP = THERD * A
50
51
         U = THERD
52
         US = FLOAT (N) * THERD
         UR = SIN (US)
53
          IF (U. EQ. 0) GO TO 30
54
55
          P3 = SIN (US)/SIN (U)
56
          P(J) = P3 * P4
57
          PDB = (20.0 * ALOG10 (ABS (P(J)/N)))
         WRITE (5, 50) X, P(J), PDB, P3, P4
58
59 50
         FORMAT (1X, SF10.6)
60
         X = X + 5.0
         WRITE (8) X, P(J), PDB
61
62
   30
         CONTINUE
63
         I = 21
64
          ENDFILE
65
          CALL PRPLOT (2, I, 8, 5, IP, DD, ID, 0)
```

66

END

